Fall 2016

Identifying shallow subsurface stratigraphy and voids using dispersive characteristics of electromagnetic and surface waves

Payman Hajiani

IDENTIFYING SHALLOW SUBSURFACE STRATIGRAPHY AND VOIDS USING DISPERSIVE CHARACTERISTICS OF ELECTROMAGNETIC AND SURFACE WAVES

by

PAYMAN HAJIANI

A DISSERTATION

Presented to the Faculty of the Graduate School of the

MISSOURI UNIVERSITY OF SCIENCE AND TECHNOLOGY

In Partial Fulfillment of the Requirements for the Degree

DOCTOR OF PHILOSOPHY

in

GEOLOGICAL ENGINEERING

2016

Approved by:

Neil L. Anderson, Advisor

Katherine R. Grote

J. David Rogers

Kelly Liu

Mohsen Asle Zaeem

PUBLICATION DISSERTATION OPTION

This dissertation consists of the following three manuscripts that have been formatted to the Missouri University of Science and Technology specifications.

Paper 1, pages 2 to 29, is entitled “Phase Shift Analysis of Surface Waves to Detect Underground Openings”, and was prepared to be submitted to the Journal of Geophysics.

Paper 2, pages 30 to 51, is entitled “Attenuation and Time-Lapse Analysis of Surface Waves to Detect Subsurface Tunnels” and was prepared to be submitted to the Journal of Applied Geophysics.

Paper 3, pages 52 to 86, is entitled “Identifying Subsurface Stratigraphy Using Dispersive Characteristics of GPR Data” and was prepared to be submitted to the Journal of IEEE Transactions on Geosciences and Remote Sensing.

ABSTRACT

This dissertation presents the results of three manuscripts on spectral analysis of electromagnetic and seismic surface waves to detect subsurface stratigraphy and voids. In the first manuscript, a new technique was developed by utilizing spectral analysis of surface waves to detect subsurface openings. This technique applied the concept of group delay to evaluate the effects of subsurface voids on the phase shift domain. Seismic data sets were acquired at different sites where the shape, size, and depth of the void varied. In all surveys, the time delay technique precisely identified the locations of the subsurface openings. The second manuscript presents the results of attenuation analyses of seismic surface waves to identify buried concrete conduits. A conduit of known size and depth was chosen for the study. Vertical and horizontal component geophones with different frequencies (14-, and 100-Hz) were employed for this study. The third manuscript presents the results of a study on dispersive electromagnetic signals to identify the thickness and dielectric permittivity of thin soil layers using Ground Penetrating Radar (GPR) techniques. Data for this experiment were acquired in a large experimental tank, where the permittivity and thickness of each soil layer was controlled. Six different experiments were carried out with three soil types, and variable-offset GPR data were acquired using four frequencies (100-, 250-, 500-, and 1000-MHz). Dispersive GPR signals were analyzed using inversion of dispersion curves to estimate the permittivity and thickness of the overlying soil layers. The accuracy of these estimates were analyzed as a function of layer thickness, antenna frequency, and permittivity. Both the thickness and permittivity estimates were most accurate when the overlying layer had a low permittivity, and higher frequencies usually had more accurate results.

ACKNOWLEDGMENTS

I would like to first thank all my committee members for their guidance and patience with me. I would like to express an especial gratitude to my adviser, Dr. Neil Anderson for his great supports and guidance. I have learned a lot under his supervisor. I would also like to thank Dr. David Rogers for his tremendous mentorship along my PhD studies. He has been a fabulous guidance and supporter not only in my research but also in my life. It would have been very hard for me to achieve my goals without his help. I would also like to thank Dr. Katherine Grote for her great advising. She was also a brilliant teacher and researcher who has guided me throughout the last project of my research. I would also like to thank Dr. Kelly Liu and Dr. Mohsen Asle Zaeem for their sincere and valuable comments on my research.

I would like to appreciate the faculty and staff of the Geological Engineering program at Missouri University of Science and Technology for their hard work.

Finally, I would like to express my enormous gratitude to my parents, brothers, and my wife,sara, for their everlasting love and support.

TABLE OF CONTENTS

Page

LIST OF ILLUSTRATIONS

Figure

PAPER I Page

PAPER II

PAPER III

LIST OF TABLES

Table

PAPER III Page

1. INTRODUCTION

Nondestructive testing methods are increasing being used to identify the subsurface features, such as thickness of soil/rock layers, physical properties, and shallow subsurface objects/anomalies that are often critical to geotechnical site characterization. Every year, underground voids such as tunnels, karst features, and abandoned mine workings. They also pose a threat to constructed infrastructure, such as the foundations of highways, railroads, pipe and transmission lines, and all types of structures. Detection of shallow underground openings, which are capable of triggering surface manifestations of collapse are in great demand, especially in areas underlain by karst or past mining activity.

In this dissertation, these manuscripts are presented. The first presents a new technique to identify the shallow subsurface tunnels. This technique involves the phase shift analysis of surface waves. The second manuscript describes the attenuation analysis of surface waves for the case of an earthen dam with a buried outfall conduit. The attenuation of Rayleigh waves and Love waves were then evaluated to see if the subsurface conduit could be reliably detected. The phase shift analysis method was also evaluated for the higher frequency geophones (100 Hz) to verify the feasibility of employing different types of geophone arrays to detect subsurface features. In the third manuscript, the dispersive characteristics of waveguides were examined. A controlled soil environment was adopted to acquire different ground penetrating radar data sets on the soil layers. The data sets for different soil textures and moisture contents were then processed and inverted to estimate the thickness and permittivity of the waveguides in the lab.

PAPER

I. PHASE SHIFT ANALYSIS OF SURFACE WAVES TO DETECT UNDERGROUND OPENINGS

Payman Hajiani, * Neil Anderson, and J. David Rogers

Department of Geosciences and Geological and Petroleum Engineering, Missouri University of Science and Technology, Rolla, MO 65401, USA

* Corresponding author.

E-mail addresses: phc5b@mst.edu (P. Hajiani), nanders@mst.edu (N. Anderson), rogersda@mst.edu (J. D. Rogers)

ABSTRACT

This paper presents the results of a new technique utilizing spectral analysis of surface waves to detect subsurface openings, such as pipes, culverts, tunnels, caverns, etc. In spite of the marked progress in nondestructive geophysical methods for detecting shallow underground voids, no unique method has emerged which can be applied globally. Seismic methods have often been employed, but they have generally been limited to the very shallow subsurface (<1.5 m). The technique presented in this study employs the concept of time delays to evaluate the presence of underground voids on the phase spectrum domain. Owing to the fact that Rayleigh waves do not propagate through air-filled voids, this study examined the phase spectrum domain to identify disturbances around subsurface openings. The results of this study have been very encouraging, insofar

that significant anomalies were noticed on the phase spectrum domains near the locations of the underground reinforced concrete culverts. Multichannel seismic surveys were performed at two locations with differing site characteristics. One survey was on asphalt concrete pavement above a concrete box culvert and the other, an earthen dam above a cylindrical concrete culvert. The overburden depths above these tunnel crowns were 1, 1.5 and 3 meters, and in all cases, the proposed time-delay technique precisely identified the depth and locations of the subsurface openings.

Keywords: Frequency domain, phase spectrum, time-lapse, void detection, wave propagation.

1. INTRODUCTION

The detection of underground cavities is of principal concern for various purposes, ranging from engineering projects to border security controls. These include such structures as buried pipes, culverts, and tunnels. Subsurface voids can be formed by natural processes, such as karst solutioning of carbonate rocks, or by human activities, such as cut-and-cover conduits, culverts, tunnels, or mining. Subsurface voids can trigger ground subsidence, damaging foundations, structures, and buried infrastructure. Detection of near-surface manmade culverts, pipelines, or tunnels is of increasing concern to security of urban infrastructures from terrorist activities, irregular warfare, and international border security.

Several experimental and numerical studies [1-9] have been undertaken to detect near-surface voids using seismic methods. Successful improvement in numerical studies of surface waves has been reported [10-12]. Each of these approaches has its own advantages and limitations. Subsurface openings cannot be detected directly from shear wave velocity anomalies [6] due to the low resolution of the inversion methods employed in Multichannel Analysis of Surface Waves (MASW) [13]. Previous studies [6] were performed to detect subsurface voids based by the diffraction of surface waves in a homogeneous half-space. The diffraction technique provided acceptable results, particularly for the synthetic examples. Unfortunately, in field situations it was almost impossible to identify the coherent diffraction patterns caused by underground openings. Cylindrical cavities generate less diffraction than rectangular voids [6, 7] and are, therefore, more challenging to identify using diffraction methods directly from the shot gather. Others have employed refraction seismic experiments to attempt detection of

cylindrical cavities [1]. However, refraction methods suffer from presence of "hidden layers," which occur when a layer of lower velocity underlies a layer of higher velocity. This is a common situation with highway pavements, where the upper layer is of a higher density, while the aggregate base or subbase is of lower density and higher porosity. Therefore, in cases such as pavements, the refraction method failed to detect underground culverts.

Numerical modeling of elastic seismic wave propagation was developed [7] to study the insitu interaction of seismic waves with near-surface voids of varying sizes and shapes. It was reported [7] that rectangular voids caused significant diffraction of incident seismic fields. Another numerical study [4] tried a quantitative method they termed "Attenuation Analysis of Rayleigh Waves" (AARW) in an attempt to detect underground openings. The results of the AARW technique suggested a promising method to locate shallow subsurface openings (< 1 m) and estimated their depths of embedment. Their study depicted the patterns of attenuation and amplification caused by constructive and destructive superposition of reflected surface waves triggered by the voids. An experimental study [14] utilized the AARW technique, which yielded similar results to previous numerical studies. However, the investigations were restricted to depths of no more than about 1m.

The multichannel analysis of surface waves (MASW) [13] technique was introduced in 1999 to evaluate insitu site characteristics, such as shear moduli of the subsurface materials (soil and/or rock), and the dispersion characteristics of the site. When an energy source is discharged, the seismic wave has to travel a certain distance before surface waves form [13]. These are termed as "near-field effects." This

phenomenon should be taken into account when dealing with data acquisition of surface waves. High frequency surface waves attenuate at a faster rate with increasing distance [15]. Consequently, at large offsets, the high-frequency components of surface waves are no longer dominant. Hence, the high-frequency components of the spectra at large offsets are then affected by body waves and direct waves [13]. These are commonly termed “far-offset effects.”

This study describes the results of spectral analysis of surface waves to detect underground openings at larger depths (~ 3 m) compared to previous studies [1, 14, 16, 17]. Two different sites were selected to perform the surveys. One was an earthen flood control dam with a cylindrical reinforced concrete spillway discharge conduit (Figure 2.1), and an asphalt concrete (A/C) pavement over a reinforced concrete box culvert (Figure 2.1.b). The sloping face of the earthen dam allowed considerable flexibility in acquiring seismic data, with a range of depths-of-cover over the discharge conduit, while the depth of cover over the concrete box culvert and A/C pavement was near constant. Various seismic data sets were acquired using multichannel receivers (vertical geophones). The wave-field was then Fourier transformed from the time domain to frequency domain. The frequency and phase spectra of the wave-field were then derived. The effects of the presence of the subsurface openings were studied on the phase spectra and the results were compared with previous studies of these same sites [14]. Remarkable anomalies in the phase-frequency domain were observed at the locations of both underground voids. The new phase spectrum methodology appears to reliably identify

both the spatial locations and the respective depths of the cylindrical and box culverts with considerable precision (+/- 0.15 m). The discussion section of this paper presents the results of the experiments in more detail.

2. DATA ACQUISITION AND METHODS

A multichannel seismograph (RAS-24^{TM}) was employed to acquire seismic data at the locations of the two reinforced concrete culverts. The cylindrical culvert beneath the earthen embankment dam is 0.91 m in diameter (Figure 2.1.a), while the concrete box culvert measured 0.70 m × 0.80 m (Figure 2.1.b). Two surveys were carried out at the earthen dam and the embedment depths (distance from the geophone spread to top of the culvert) were set 1.52 m and 3.05 m. The embedment depth at the box culvert and asphalt concrete pavement site was 1 m. A 9 kg sledgehammer and base plate were utilized to deliver the impact seismic source. The shots were acquired with different source-receiver offsets to control the near and far-offset affects. At each source location, 3 to 5 shots were acquired and vertically stacked to suppress ambient noise. Vertical geophones with 4.5 Hz eigenvalues were employed to record the vertical components of the seismic data sets. The total recording time was set long enough (1-1.5 seconds) so the entire surface wave forms recorded by the last channels. Figure 2.1.c shows a typical offset-time representation of acquired seismic data in a near-surface application (the data set was acquired at the asphalt pavement site). The source-receiver offset was 4.6 m (Figure 2.1.c) and the total recording time was 1000 ms, which was truncated to 350 ms in the processing step for display purposes. The real amplitudes of the signals were normalized with respect to the highest amplitude recorded in each trace.

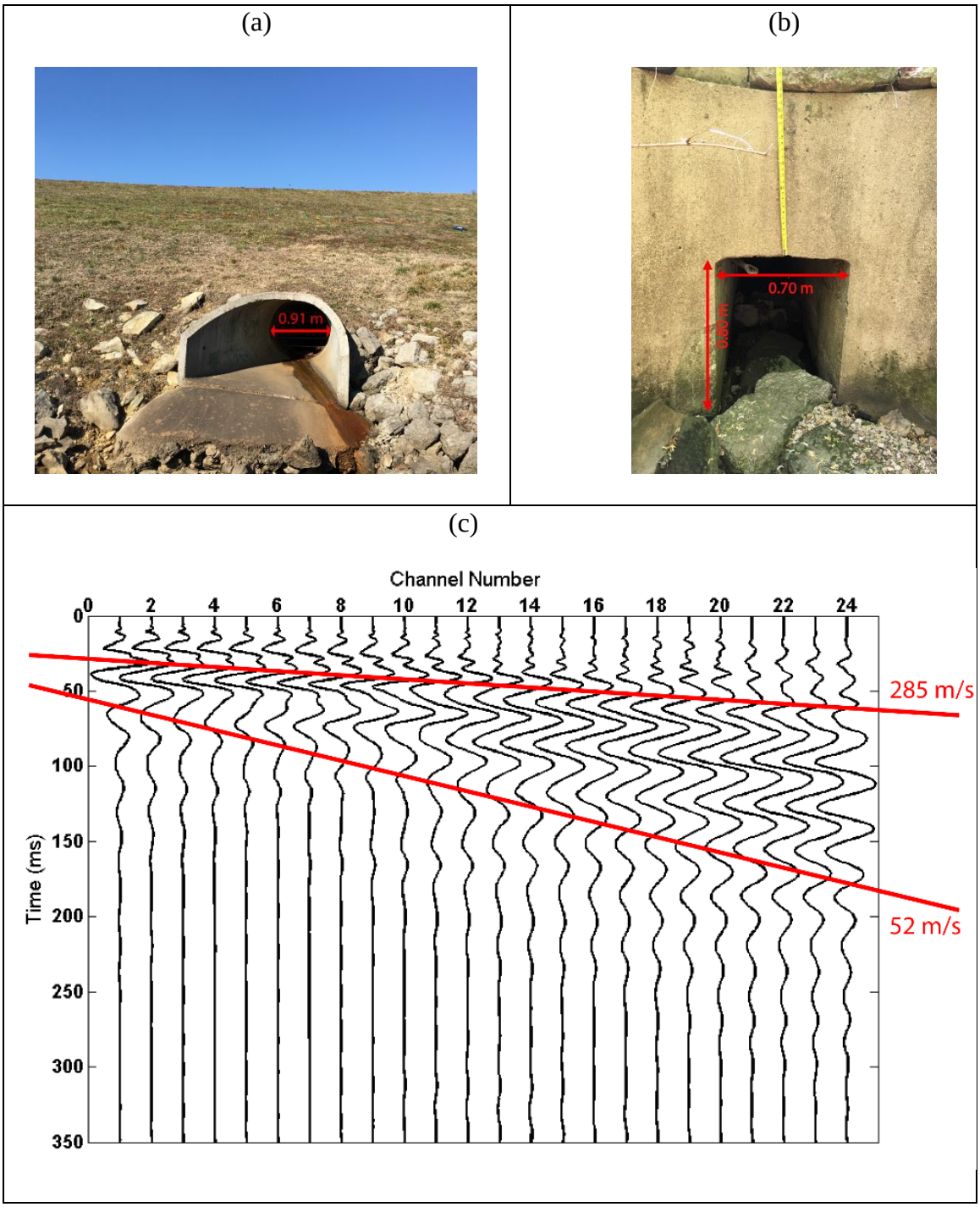

Figure 2.1. (a) and (b) Images of the earthen dam with the cylindrical concrete culvert and the concrete box culvert beneath asphalt concrete pavement, respectively. (c) a 24-channel seismic time-space profile acquired for the concrete box culvert. Two linear events are velocities of dispersive Rayleigh waves.

In order to reduce the far-offset effects (discussed in the introduction section), direct waves, air waves, and body waves (which arrive before the Rayleigh waves) were filtered out on the shot gather profile (Figure 2.1.c). This filtering process is an important step in this method to increase the signal-to-noise ratio at far offsets. Equally important, the geophone spreads were set relatively short (0.30 m geophone spacing) to degrade the influence of body waves on the surface waves at large offsets [18].

Rayleigh waves can be identified on the shot gather (Figure 2.1.c) by their relatively higher amplitudes, coherent patterns, and arrival times. Other unwanted signals, such as direct waves, air waves, reflections, and refraction waves, can also be filtered out. In a shot gather, direct waves and refracted rays are always the first breaks (first arrivals). Even though the geological reflectors (i.e. horizontal layers) have small reflection coefficients, reflection waves are normally of low amplitudes, and are often masked by the higher amplitude surface waves.

Three shots were acquired at each source station and vertical stacking procedures were applied in order to cancel out the incoherent ambient noise and improve the signal-to-noise (S/N) ratio. As the first step, the Attenuation Analysis of Rayleigh Waves (AARW) [4] was applied to the acquired multichannel seismic data.

In this study, an additional processing step was employed before performing the AARW algorithm. This step included an f-k filter to remove the unwanted waves, such as ambient cultural noise, direct P-waves, refracted waves, reflection, and air waves on the shot gather. These unwanted waves were considered noise in this study. Figure 2.1c presents a typical seismic shot gather and the surface waves that are retained for the

AARW method. The surface waves attenuate faster than body waves at large offsets, therefore, filtering of the unwanted signals should improve the AARW technique.

Next, a Discrete Fourier Transform (DFT) technique was applied on the acquired seismic data (time series) to extract the frequency components of the wave fields. Once the frequency spectra were acquired, Normalized Energy-Distance (NED) [14] parameters could be calculated. Since the purpose of this study was to examine the attenuation of surface waves due to the existence of underground voids, a gain function was applied across the array in order to compensate for the geometrical damping [4, 14]. The cumulative signal energy was calculated at each geophone station according to the following equation:

$$E_i = \sum_{f=0}^{f_N} \left| A_f \right|^2 \tag{1}$$

where E_i is the cumulative signal energy at station i, the summation performed over the whole frequency range, and A_f is the amplitude of the spectrum at frequency component f.

Then, the Normalized Energy Distance (NED) parameters were computed across the array at each geophone station:

$$NED_i = E_i \Big/ max(E_i) \tag{2}$$

The energy spectrum was then normalized to the maximum energy that existed across the array. Figure 2.2 presents the NED plots for the earthen dam with 1.52 and 3.05m depths from the array to the crowns of the culverts.

The results of this study appear to verify a useful technique to detect the presence of subsurface culverts or tunnels to depths up to at least 3m. First, the phase spectra

corresponding to the frequency components of the wave field were extracted. Then, the phase spectra for each channel were unwrapped so that the changes in the slope of the phase shift could be studied. Group delay, mathematically, is the negative derivative of the phase with respect to frequency [19], and is measured in radians/Hz. Figures 3.1 and 3.2 show the phase shifts of different channels for the shot gather acquired at the earthen dam and the asphalt concrete pavement site. The reader should note that useful information can be drawn from the unwrapped phase spectrum plots. The changes in the slope of the phase shifts can be traced, and the time delays then studied.

Various shot gathers at both sites with different embedment depths (depth form the survey line to the top of the void) were processed and the corresponding phase spectrum plots were extracted. Typical results can be seen in Figures 3.1 and 3.2. The following section presents the summary of findings and the Discussion section explains the feasibility of the time delay technique for detecting near-surface voids.

(a)

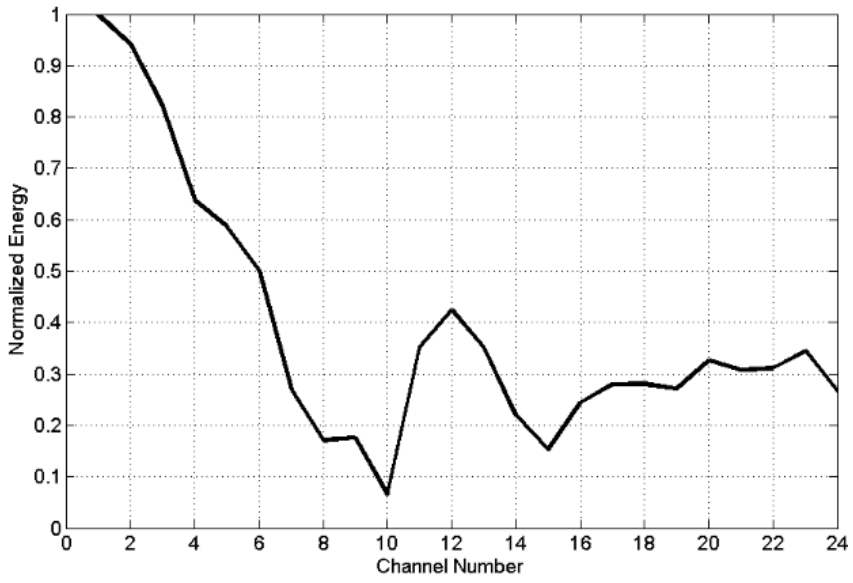

(b)

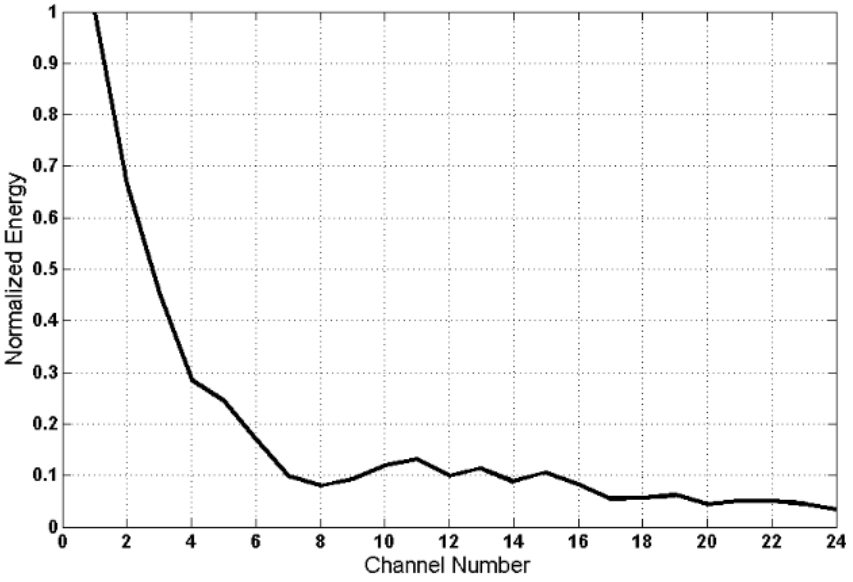

Figure 2.2. Normalized Energy Density plots for the seismic data acquired on the earthen dam. (a) 1.52 m depth to the top of the box culvert. (b) 3.05 m depth to the top of the circular culvert.

3. RESULTS

Normalized Energy-Distance (NED) parameters were calculated and plotted for the earthen dam and the A/C pavement. Different source-receiver offsets were considered at both locations. Also, different embedment depths were considered at the earthen dam site. Figure 2.2 presents the NED parameters for the earthen dam, where (a) the center of the concrete box culvert is located between channels 11 and 12, and the depth from the array to the top of the tunnel is 1.52m. Figure 2.2.b is taken at the center of the cylindrical concrete culvert (tunnel), between channels 9 and 10, with an embedment depth of 3.05m.

Next, multi-mode dispersion images were developed from the shot gathers. The dispersion image extraction used in this study was based on the Wakefield transformation method [18]. Figure 3.1 presents the results for the dispersion-curve images and the phase shift plots of the earthen dam site. Figures 3.1.a and 3b show the results of the experiments for the embedment depths of 1.52 m where the spillway was centered beneath channel numbers 11 and 12 of the geophone spread. Likewise, Figures 3.1.c and 3d show the processed data for the same earthen dam at an embedment depth of 3.05 m. In the latter case, the geophone spread was positioned intentionally, for comparison purposes, such that the center of the spillway lay beneath channels 9 and 10 of the geophone spread. The dispersion-curve image for the 1.52 m embedment depths consist of the fundamental and the higher mode. The fundamental mode ranges from 20 to 60 Hz and the higher mode ranged between 60 and 110 Hz. On the other hand, the fundamental mode ranged between 30 and 80 Hz for the 3.05 m embedment depth (Figure 3.1.c). The higher mode is clearly indicating the frequency range of between 80 and 140 Hz.

The same procedure was then applied to obtain the dispersion images and the phase spectra for different shot gathers at the A/C pavement site. Figure 3.2.a illustrates the dispersion characteristics of the Rayleigh waves from the shot gather acquired on the A/C pavement site. The fundamental mode is clearly separated from the higher modes. Additionally, the energy for the fundamental mode is easily distinguished in a desirable frequency range (20-70 Hz). Figure 3.2.b, on the other hand, illustrates the changes of the phase spectrum with respect to frequency (time delay) for the same shot gather. The phase spectrum has been unwrapped to track the changes of phase spectrum, with respect to frequency for each trace. The changes in slopes and anomalies in the slopes can be seen from the phase shift plots (Figures 3.1.b, 3.1.d, and 3.2.b).

It is necessary to realize that data acquisition plays an important role in the final results. Ambient noise can adversely affect the S/N ratio, and consequently, the phase-shift plots can be contaminated with unwanted signals. The next section discusses the results and their significance.

4. DISCUSSION

To date, the AARW method has only been useful in detecting voids in the very shallow subsurface, usually depths of less than 1.5 m. This physical limitation can be appreciated in Figure 2.2, which demonstrates the impacts of increasing the embedment depth from 1.52 to 3.05m. The AARW method was unable to detect anomalies over the concrete culvert for the deeper case (Figure 2.2.b). However, small ripples over the location of the culvert are still present and they suggest the presence of a reflector at greater depth. Numerical modeling [4] and experimental studies [14] suggest that AARW is a powerful method to detect the location and embedment depth of shallow voids (less than 1.5 m). Previous studies [14] successfully detected the same spillway (at the earthen dam site) at a shallower depth of 0.9 m, whereas in this study, the AARW method successfully detected the location of the void with an embedment depth of 1.52 m (Figure 2.2.a). This experiment appears to be a compelling evidence that filtering out the unwanted signals, such as the refracted waves, direct waves, etc., can improve the signal-to-noise ratio for the study of surface wave attenuation. As a result, the AARW method displays a more explicit anomaly over the location of the same culvert, but with a deeper embedment depth.

As mentioned previously, Rayleigh waves are not able to propagate through air-filled voids due to the fact that the shear modulus for air is zero. As a consequence, it is assumed that a time delay in Rayleigh waves occurs wherever air-filled voids are present. In considering the dispersion characteristics of surface waves, it appears that only select frequencies of surface waves penetrate to the depth where the void exists. Therefore, Rayleigh waves with those frequency ranges could be expected not to propagate through

the air-filled voids. The same is true for the water-filled voids because the shear moduli for liquids are zero as well. Owing to the fact that shear waves do not propagate in air, a time delay would be expected to be observed in the proximity of the location of the void in the phase-frequency domain.

In addition, reflection of seismic waves from the void interfaces cause disturbances in certain frequency ranges of the phase-frequency spectra. The reason is that only certain frequencies (wavelengths) of the Rayleigh waves penetrate to the depth where the voids exist and thereby interact with the void boundaries. At this juncture, some portion of the incident waves reflect back to the medium, while other portions are diffracted and transmitted. These reflected waves superpose with the incident waves. The wave interactions can be constructive or destructive, leading to a shift in amplitudes and phases. A previous study [4] verified the regions of amplification and attenuation between the energy source and the air-filled voids.

Dispersion-curve images (Figure 3.1 and 3.2) exhibit different modes and the corresponding frequency bandwidths. For the seismic data acquired at the earthen dam with the 1.52 m embedment depth, the fundamental mode (Figure 3.1.a) is dominant over the frequency range of 20-60 Hz. The phase spectrum (Figure 3.1.b) reveals an anomaly over the channel numbers 10 to 13 at frequencies of 40 Hz and above. By these means, the anomaly can successfully identify the location of the buried concrete conduit.

In the case of the 3.05 m embedment depth at the earthen dam (Figure 3.1.c), the fundamental mode corresponds to the frequency range of 30-80 Hz, and the higher mode is dominant in the frequency range of 80-140 Hz. According to [20], higher modes carry higher energies compared to the fundamental modes. Higher modes also correspond to

the higher frequencies and the far higher phase velocities. For these reasons, Rayleigh waves associated with the higher modes area able to propagate to greater depths. In other words, higher modes can identify anomalies at greater depths. However, Figure 3.1.d reveals that the phase spectra anomaly occurs in vicinity of channels 9 to 11 in the frequency range of 42-48 Hz), which appears to be the fundamental mode. The anomaly in the unwrapped phase spectrum successfully identified the location of the reinforced concrete culvert boundaries.

A third set of surveys were performed on the asphalt concrete (A/C) pavement, where it passes over a reinforced concrete box culvert. The geophone spread was positioned in a way so that the concrete box culvert was centered beneath channels 6 to 8. The depth to the top of the culvert was 1.22 m. Figure 3.2.a shows that the fundamental mode is dominant in the wide frequency range of 20-80 Hz. Accordingly, the anomaly in the phase spectrum (Figure 3.2.b) began with channel number 6 and contains the frequency range of 40 to 80 Hz. The disturbance in the phase spectrum successfully identified the horizontal location of the concrete box culvert. It should be noted that the phase shift plots exhibited wave healing for the channels to either side of the voids. In other words, the slope of the phase shift against frequency became increasingly coherent with the neighboring channel time delays (Figure 3.1).

It is important to note that filtering out the body waves is crucial to using this Time Delay method. Once the body waves were filtered out, the phase spectrum highlighted the time delay due to the existence of the air-filled void. It was noticed that without filtering the unwanted signals (and only retaining the surface wave energies in the shot gather), the phase-frequency domain reveals no anomaly, even if the voids were

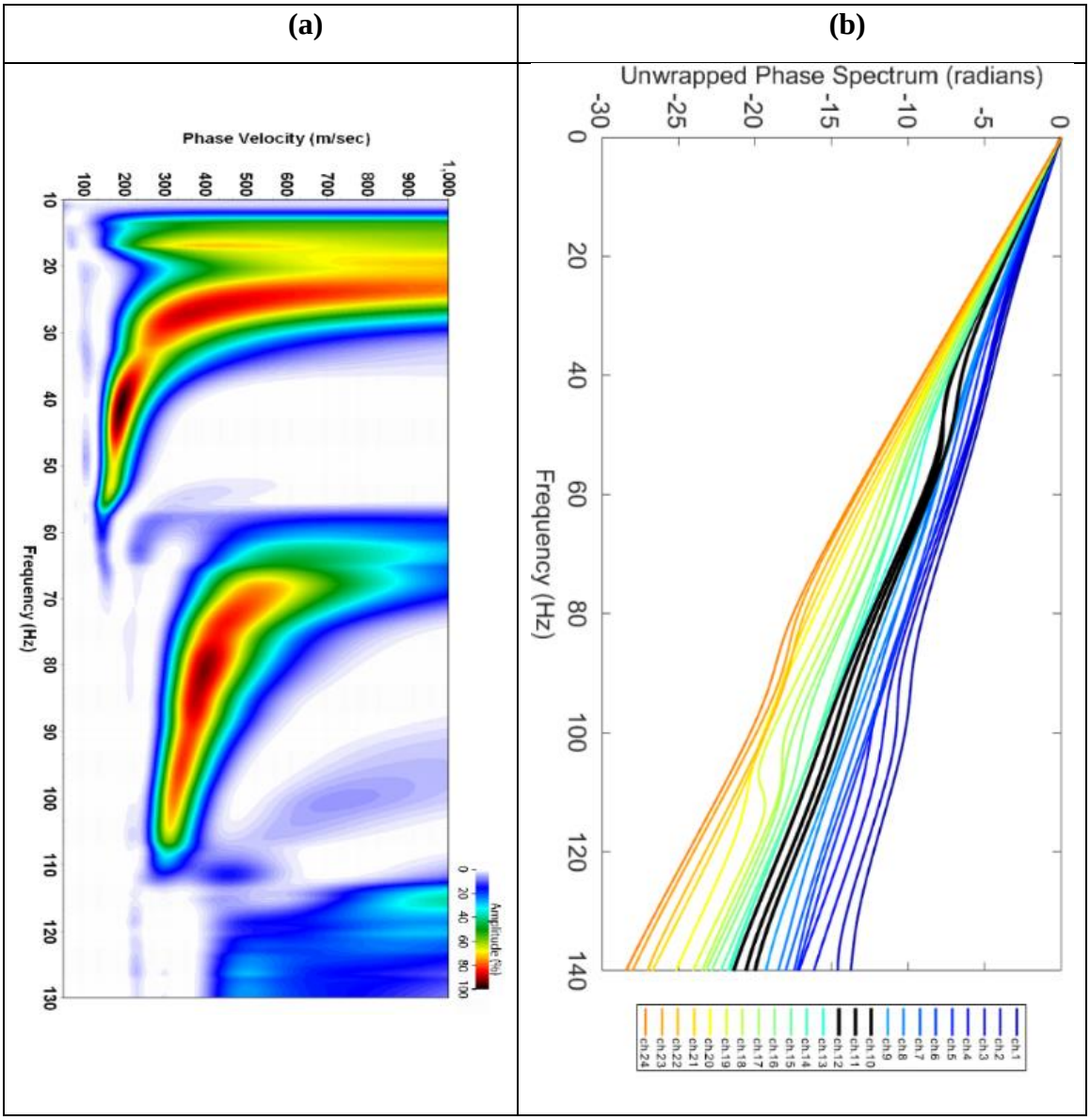

Figure 4.1. (a) and (b) show the dispersion image and the unwrapped phase spectra for the earthen dam with the 0.91 m diameter culvert. The embedment depth (depth from the survey line to the top of the tunnel) is 1.52 m and the center of the tunnel positioned beneath channels 11 and 12 of the survey. (c) and (d) are related to the same earthen dam, but where the embedment depth was increased to 3.05 m and the survey line positioned so that the center of the tunnel *was* beneath channels 9 and 10.

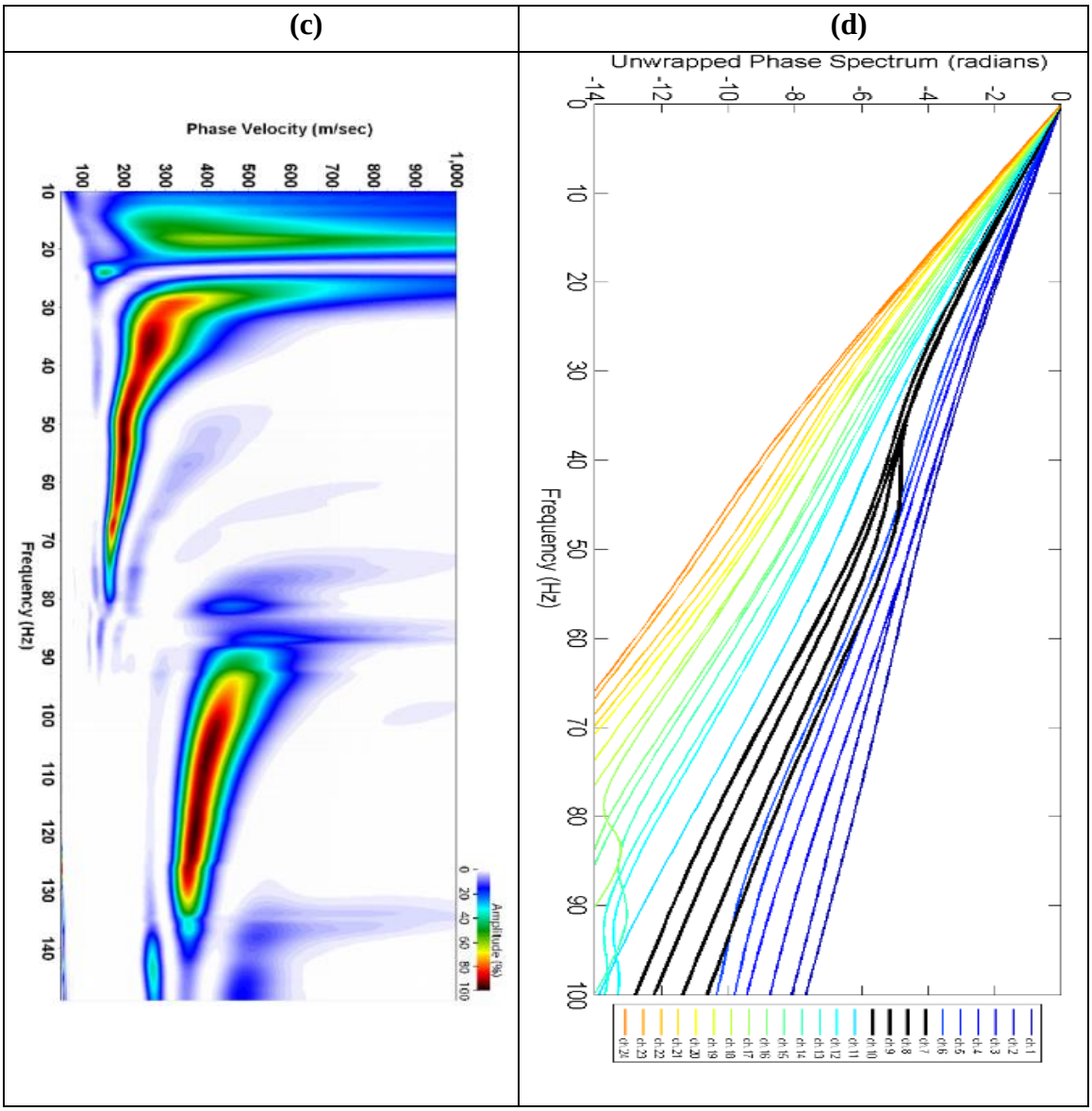

Figure 4.1. (a) and (b) show the dispersion image and the unwrapped phase spectra for the earthen dam with the 0.91 m diameter culvert. The embedment depth (depth from the survey line to the top of the tunnel) is 1.52 m and the center of the tunnel positioned beneath channels 11 and 12 of the survey. (c) and (d) are related to the same earthen dam, but where the embedment depth was increased to 3.05 m and the survey line positioned so that the center of the tunnel *was* beneath channels 9 and 10. (Cont.)

present. In fact, the slopes of the phase spectra changed (time delay) gradually for each channel when no filtering was applied. The reason is that the first arrivals (direct waves and the critically refracted waves) arrive at the geophone stations without being influenced by the void, because of its depth. Because of this, no time delay is observed. In general, the direct waves and the critically refracted waves (if any) arrive at the stations in order, and therefore, without filtering them out, the slope in the phase shift presents a constant and gradual change, so that (no anomaly can be observed.

It is important to note that filtering out the body waves is crucial to using this Time Delay method. Once the body waves were filtered out, the phase spectrum highlighted the time delay due to the existence of the air-filled void. It was noticed that without filtering the unwanted signals (and only retaining the surface wave energies in the shot gather), the phase-frequency domain reveals no anomaly, even if the voids were present. In fact, the slopes of the phase spectra changed (time delay) gradually for each channel when no filtering was applied. The reason is that the first arrivals (direct waves and the critically refracted waves) arrive at the geophone stations without being influenced by the void, because of its depth. Because of this, no time delay is observed. In general, the direct waves and the critically refracted waves (if any) arrive at the stations in order, and therefore, without filtering them out, the slope in the phase shift presents a constant and gradual change, so that (no anomaly can be observed.

When the source-to-underground void offset was relatively short (~ 5.5 m), the impact on phase spectrum was relatively weak and unable to identify the buried culverts. According to Park et al., [13] different frequency components of the seismic wave must

travel at least half their wavelength distance before these frequency components can be established (near-field effects).

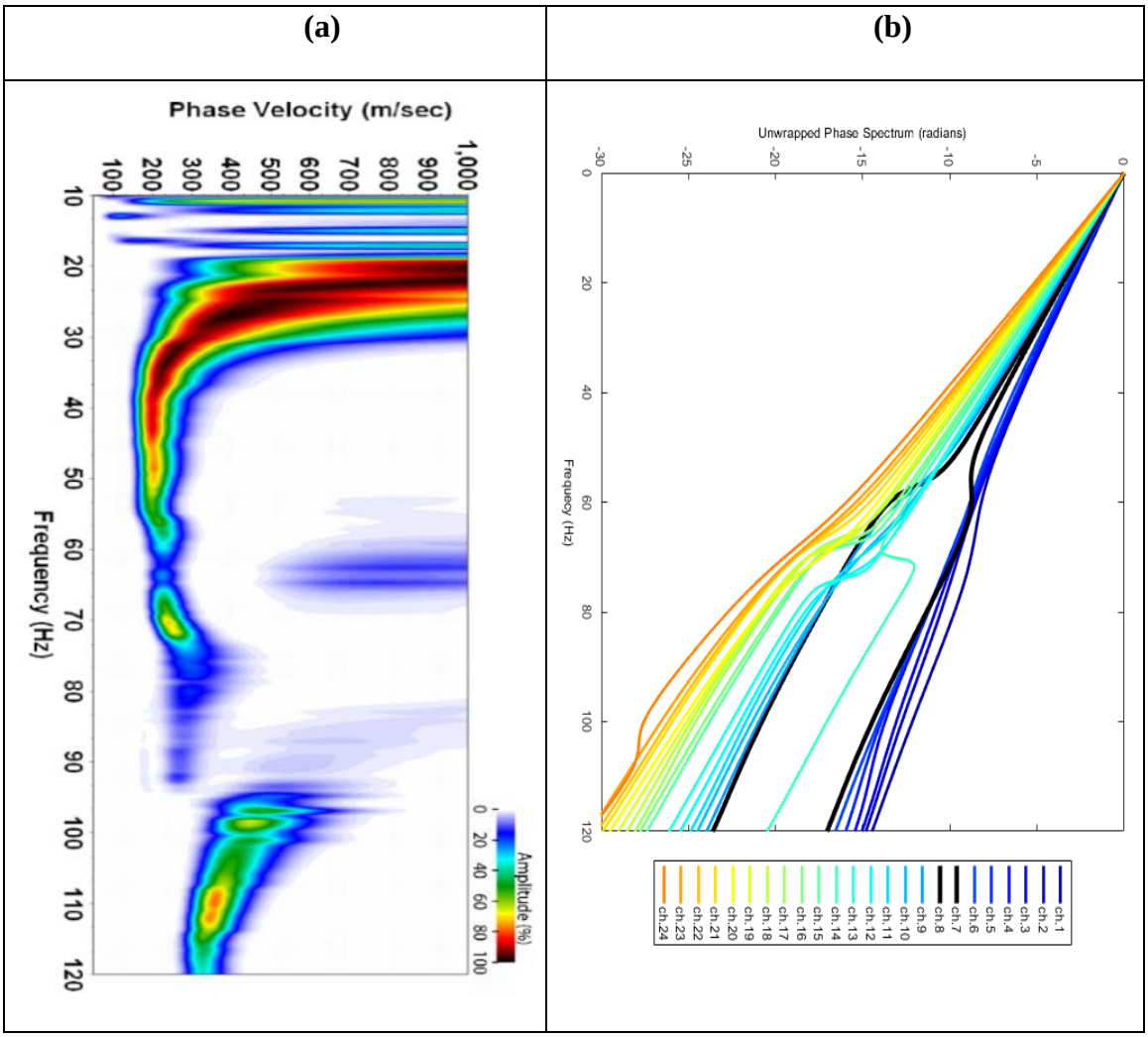

Figure 4.2. (a) Dispersion image (velocity spectrum) obtained from the shot gather in Figure 2.1 using SurfSeis™ software (KGS). (b) Unwrapped phase spectrum with respect to frequency of the same shot gather from Figure 2.1.

Therefore, when the source-to-underground void offsets are relatively short, certain wavelengths have not been developed before interacting with the boundaries of

the void. It is, therefore, practical to perform some seismic surveys, and then, based on the dispersion images, determine the best geometries of the survey; such as source to first receiver offset and the geophone spread length.

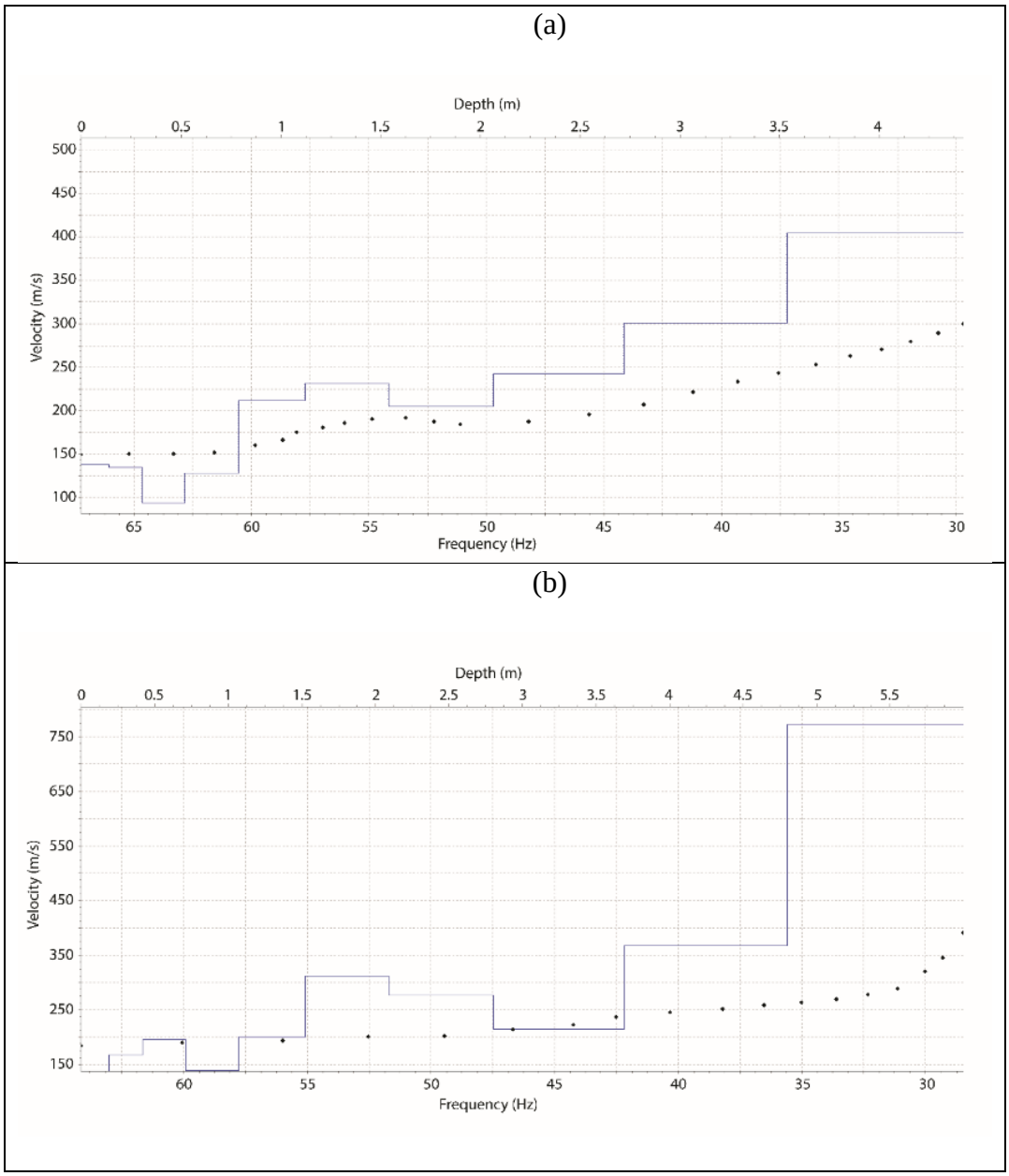

Figure 4.3. Shear wave velocity profiles. (a) the concrete culvert 1.52 m deep within an embankment dam. (b) the same concrete culvert at a depth of 3.05 m. (c) the concrete box culvert 1 m beneath the A/C pavement. Dotted lines represent the fundamental dispersion curves.

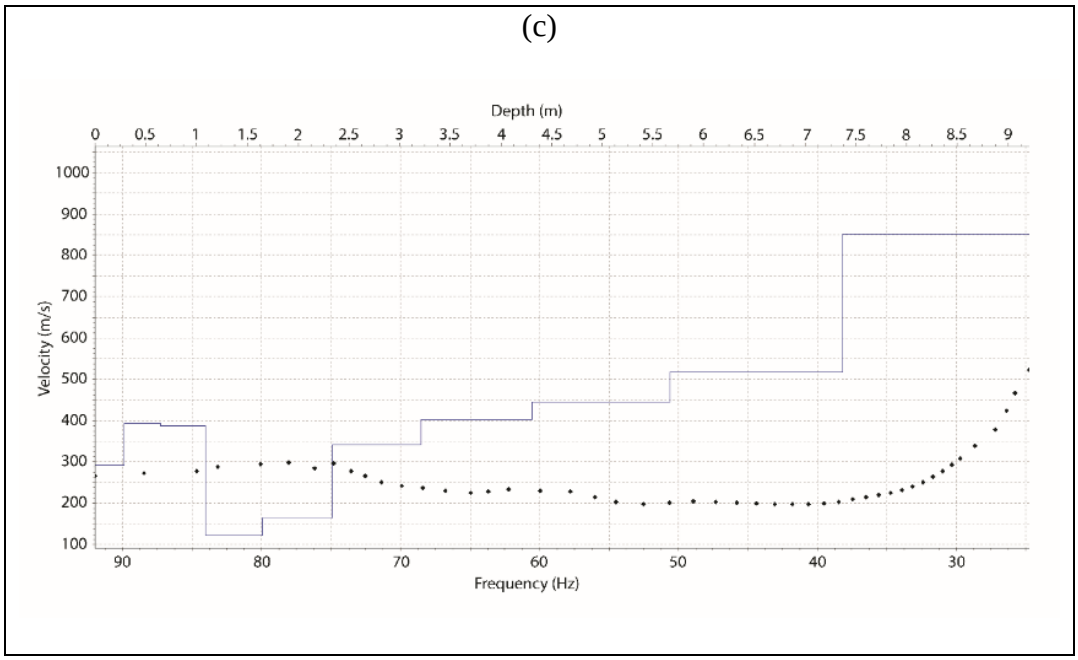

Figure 4.3. Inverted Shear wave velocity profiles. (a) the concrete culvert 1.52 m deep within an embankment dam. (b) the same concrete culvert at a depth of 3.05 m. (c) the concrete box culvert 1 m beneath the A/C pavement. Dotted lines represent the fundamental dispersion curves. (Cont.)

It is also important to keep the receiver spacings short to obtain a higher spatial resolution. It is also recommended to set the total recording time long enough to obtain a higher frequency resolution. Otherwise, if the sample rate is not high enough, unwrapping the phase spectrum might be impossible. The MATLAB program used in this study unwraps the phases by changing absolute jumps of equal or greater than π to their 2π complements. As a result, to keep the jumps relatively small, there needs to be large number of data points (number of samples in the frequency domain) on the phase spectrum plots. It is recommended that total recording times of 1 second or longer be employed. However, long recording times can also decrease the N/S ratio.

In final consideration, Figure 4.3 shows the shear wave velocity profiles for the site locations of this study. These 1-D shear wave velocity profiles were attained using

the inversion methods developed previously [13, 20], based on the multichannel analysis of surface waves (MASW).

To emphasize, these S-wave profiles represent the average shear wave velocities of the shallow subsurface units lying beneath the geophone spreads. The solid lines display the layer depths and the corresponding shear wave velocities. It is generally expected that with increasing in depth the shear wave velocity increases as well. However, sometimes a layer with a low shear wave velocity layer can lie beneath higher shear wave velocity layers. With attention to the fact that the inverted S-wave velocity profiles (Figure 4.3) represent only the average velocities of the subsurface layers, it can be seen that the shear wave velocity drops on the inversion plots coincide at depths where the voids were present. Notably, for the cylindrical concrete culvert beneath the earthen dam with 1.5 m embedment depth, the average of the shear wave velocity drops from 230 m/s to 200 m/s (Figure 4.3.a). Similarly, for the same concrete culvert with the 3.05 m embedment depth, the inversion (Figure 4.3.b) shows a drop of 70 m/s in shear wave velocity at 2.8 m depth. As can be seen, a similar drop in shear wave velocity occurred for the A/C pavement inversion plot, but with a greater drop in velocity. Since the layers of the A/C pavement were already compacted, the shear wave velocity of the upper layers are very high. Because of this, the drop in the average shear velocity of the layer containing the concrete box culvert was also greater.

It appears that the phase-frequency domain and the method of “time delay” is a promising technique to estimate the horizontal location and depth to the subsurface voids with significant precision to depths of at least 3 m.

5. CONCLUSIONS

In this study, the effects of filtering out the unwanted signals (direct waves, air waves, etc.) showed a significant improvement over the AARW method for detecting deeper near-surface voids. The study also revealed that the AARW technique was not able to identify the presence of voids when the embedment depths were deeper than ~ 1.5 m.

This study evaluated the feasibility of detecting near-surface voids based on the phase-frequency spectrum domain. A change in the slope of the phase-shift versus frequency indicates a time delay. Since the shear modulus for air is zero, shear waves do not propagate through air-filled voids. This allowed identification of a time-lapse on the phase spectrum domain. The process of filtering out the unwanted signals (waves rather than surface waves) which arrive before the surface waves was necessary to ensure that only the time-lapse of the surface waves be monitored. In other words, only the interaction of the surface waves and the voids should be analyzed.

The dispersive characteristics of the Rayleigh waves ensure that different frequencies (wavelengths) propagate to different depths. Therefore, only frequencies (wavelengths) of certain values will interact with the voids. The application of time delays on the surface waves appears to be a promising technique for detecting near-surface voids, pipes, culverts, and tunnels when the AARW technique cannot sense deep voids deeper than 1.5 m.

Further experimental and numerical studies are suggested to evaluate the functionality of the time-lapse technique for voids with different sizes and embedment depths.

ACKNOWLEDGMENTS

The authors would like to thank Adel Elkrry and Stanley Nwokebuihe for their help in data acquisition. We also would like to express our appreciation for Dr. Kurt Kosbar's comments and review. This research did not receive any specific grant from funding agencies in the public, commercial, or not-for-profit sectors.

REFERENCES

[1] Engelsfeld T, Šumanovac F, Pavin N. Investigation of underground cavities in a two-layer model using the refraction seismic method. Near Surface Geophysics. 2008;6:221-31.

[2] Grandjean G, Leparoux D. The potential of seismic methods for detecting cavities and buried objects: Experimentation at a test site. Journal of Applied Geophysics. 2004;56:93-106.

[3] Leparoux D, Bitri A, Grandjean G. Underground cavity detection: A new method based on seismic Rayleigh waves. European Journal of Environmental and Engineering Geophysics. 2000;5:33-53.

[4] Nasseri-Moghaddam A, Cascante G, Hutchinson J. A new quantitative procedure to determine the location and embedment depth of a void using surface waves. Journal of Environmental and Engineering Geophysics. 2005;10:51-64.

[5] Sloan SD, Peterie SL, Miller RD, Ivanov J, Schwenk JT, McKenna JR. Detecting clandestine tunnels using near-surface seismic techniques. Geophysics. 2015;80:EN127-EN35.

[6] Xia J, Nyquist JE, Xu Y, Roth MJS. Feasibility of detecting voids with rayleigh-wave diffraction. 19th Symposium on the Application of Geophysics to Engineering and Environmental Problems, SAGEEP 2006: Geophysical Applications for Environmental and Engineering Hazzards - Advances and Constraints2006. p. 1168-80.

[7] Gelis C, Leparoux D, Virieux J, Bitri A, Operto S, Grandjean G. Numerical modeling of surface waves over shallow cavities. Journal of Environmental and Engineering Geophysics. 2005;10:111-21.

[8] Tran KT, McVay M, Faraone M, Horhota D. Sinkhole detection using 2D full seismic waveform tomography. Geophysics. 2013;78:R175-R83.

[9] Shao GZ, Tsoflias GP, Li CJ. Detection of near-surface cavities by generalized S-transform of Rayleigh waves. Journal of Applied Geophysics. 2016;129:53-65.

[10] Cho YS, Lin F-B. Spectral analysis of surface waves in single and multi-layer slabs with finite thickness using finite element modelling. NDT & E International. 2005;38:195-202.

[11] Chai HY, Phoon KK, Goh SH, Wei CF. Some theoretical and numerical observations on scattering of Rayleigh waves in media containing shallow rectangular cavities. Journal of Applied Geophysics. 2012;83:107-19.

[12] Saikia A. Numerical study on screening of surface waves using a pair of softer backfilled trenches. Soil Dynamics and Earthquake Engineering. 2014;65:206-13.
[13] Park CB, Miller RD, Xia J. Multichannel analysis of surface waves. Geophysics. 1999;64:800-8.

[14] Putnam NH, Peng X, Cawlfield JD, Kovin ON, Torgashov EV, Modur P, et al. Attenuation analysis of Rayleigh waves used to locate shallow manmade tunnels. 43rd US Rock Mechanics Symposium and 4th US-Canada Rock Mechanics Symposium2009.

[15] Bullen KE, Bolt BA. An introduction to the theory of seismology. Fourth edition. An introduction to the theory of seismology Fourth edition. 1985.

[16] Nasseri-Moghaddam A, Phillips C, Cascante G, Hutchinson DJ. Detection of underground cavites using MASW test. 33rd CSCE Annual Conference 2005. Toronto, ON2005. p. GC-270-1-GC-270-11.

[17] Xia J, Xu Y, Miller RD, Nyquist JE. Rayleigh-wave diffractions due to a void in the layered half space. SEG Technical Program Expanded Abstracts2006. p. 1406-10.

[18] Park CB, Miller RD, Xia J. Imaging dispersion curves of surface waves on multi-channel record. 68th Ann Internat Mtg, Soc Expl Geophys1998. p. 1377-80.

[19] Venghaus H. Wavelength Filters in Fibre Optics: Springer Berlin Heidelberg; 2006.

[20] Xia J, Miller RD, Park CB, Tian G. Inversion of high frequency surface waves with fundamental and higher modes. Journal of Applied Geophysics. 2003; 52:4557.

II. ATTENUATION AND TIME-LAPSE ANALYSIS OF SURFACE WAVES TO DETECT SUBSURFACE TUNNELS

Payman Hajiani, * Neil Anderson, and J. David Rogers

Department of Geosciences and Geological and Petroleum Engineering, Missouri University of Science and Technology, Rolla, MO 65409, USA

* Corresponding author.

E-mail addresses: phc5b@mst.edu (P. Hajiani), nanders@mst.edu (N. Anderson), rogersda@mst.edu (J. D. Rogers)

ABSTRACT

The detection of underground cavities is of significant concern to geotechnical engineers working in karst terrain, or those searching for tunnels or buried utilities. In spite of the marked progress in nondestructive geophysical methods for detecting shallow underground voids, no unique methodology has emerged that can be applied globally. Various studies have been performed using Rayleigh waves to detect shallow tunnels. In this study, the feasibility of detecting shallow (<4 m) subsurface tunnels by employing attenuation analysis of Rayleigh and Love waves were examined. Vertical geophones with Eigen-frequencies of 4.5 Hz, 14 Hz, and 100 Hz were utilized to evaluate Rayleigh waves to detect the depth and diameter of near-surface tunnels. Seismic surveys were carried out using horizontal 14 Hz geophones to verify the feasibility of using Love waves to detect shallow tunnels and buried conduits. An embankment dam 10 m high with an outfall conduit was selected for evaluation. Attenuation analyses of surface waves were performed

on all of the data sets to see if we could detect the buried conduit beneath various depths of soil cover, up to 3.8 m depth. An amplification of energy on, or in front of the near boundary of the conduits was thereby observed, indicating seismic reflection from the interface of contrasting densities. However, time delay analysis confirmed the presence of void causing the surface waves to propagate with a delay. The results of this study not only confirmed the validity of time delay technique in detecting air-filled voids, but also displayed the ability of Love waves to detect shallow subsurface tunnels or buried conduits.

Keywords: Frequency domain, Love waves, phase spectrum, time-lapse, void detection.

1. INTRODUCTION

Detecting subsurface voids is of great importance to many different engineering projects. Abandoned mines, karst features, and covert tunneling can cause major problems to constructed infrastructure, as well as structural foundations.

Various studies have been reported that sought to detect shallow subsurface voids, including those using scattered guided waves (Herman et al., 2000), surface waves (Grandjean and Leparoux, 2004; Nasseri-Moghaddam et al., 2005b; Xia et al., 2007; Xia et al., 2012; Xia et al., 2006), attenuation analysis (Nasseri-Moghaddam et al., 2005a; Putnam et al., 2009), phase shift analysis (Hajiani et al., currently in review), numerical studies (Frehner et al., 2008; Gelis et al., 2005; Nasseri-Moghaddam et al., 2007), surface wave diffraction (Xia et al., 2007; Xia et al., 2006; Zeng et al., 2009), refraction seismic method (Engelsfeld et al., 2008; Nolan et al., 2011). Each technique exhibits intrinsic advantages and disadvantages. For example, multichannel analysis of surface waves (MASW) analyzes the average shear wave velocity of different subsurface layers under the geophone spread (Park et al., 1999; Park et al., 1998). Therefore, heterogeneities, such as a small conduit (< 2 m in diameter) do not show anomalies on the shear wave profile. Moreover, refraction methods are most useful in layered subsurface strata, were the shear wave velocity of the layers typically increases with depth. Otherwise, the refracted waves do not form. Phase shift analyses are very susceptible to the presence of noise, and changes in the phase shifts can be disturbed by the presence of noise. However, noise removal techniques can enhance the abilities of this technique. Shear wave velocity profiles obtained from MASW profiles have not provided useful information for detecting subsurface openings (Xia et al., 2006). The Rayleigh wave

diffraction method advanced by Xia et al. (2006) was unsuccessful in detecting circular openings less than 2m in diameter.

Park et al. (1999) demonstrated that multichannel analysis of surfaces waves (MASW) presented an efficient means of acquiring and processing the surface waves using laptop computer technology. According to Park et al. (1998), an anomaly in shear wave velocity occurs when a part of the medium has significantly different elastic properties as compared to the surrounding strata. This is partially because surface waves are dispersive in an inhomogeneous medium (Xia et al., 1999). Furthermore, longer wavelengths are sensitive to the elastic properties of the deeper layers, whereas shorter wavelengths are sensitive to elastic properties of shallower subsurface materials. Therefore, dispersive Love waves and Rayleigh waves provide useful information from different depths of the subsurface.

In this study, attenuation analysis of Love waves and Rayleigh waves were carried out. Three different geophone types (100 Hz vertical, 14 Hz horizontal, and 14 Hz vertical) were employed to study the attenuation of surface waves. The method used in this study is based on the attenuation analysis of Rayleigh waves (AARW) developed in previous studies (Nasseri-Moghaddam et al., 2005a; Putnam et al., 2009). An embankment dam with an outfall conduit of known size and embedment depth allowed us to evaluate the utility of new techniques with increasing depth of cover (up to 4.1m). In addition to the attenuation analysis of surface waves, a time-lapse analysis of surface waves was also performed on the higher frequency geophones (100 Hz) to compare the results with the previous studies (Hajiani et al., currently in review).

The results of this study are described in the results section without interpretation so that readers can develop their ideas and models based on the obtained (raw) results. The discussion section then describes the attenuation analyses of both Love waves and Rayleigh waves.

2. DATA ACQUISITION AND METHODS

In this study, a reinforced concrete conduit of known size and embedment depth was selected. The conduit serves as a spillway outfall for an embankment dam (Figure 2.1.a). Three sets of geophones were employed: vertical 14 Hz, horizontal 14 Hz, and vertical 100 Hz.

20 horizontal geophones (14 Hz) were employed to acquire Love waves 3.8 m above the conduit. The geophones axes were set perpendicular to the geophones array (Figure 2.1.b) and a shear source (Figure 2.1.c) was adopted to generate Love waves. The vertical distance between the survey line and the top to the spillway was set at 3.8 m for both vertical and horizontal 14 Hz geophone surveys. The spacing between geophones was set at 0.6 m, and a 9 kg sledgehammer discharged the metallic plate source. A multichannel seismograph (RAS-24^{TM}) recorded the seismic data sets. The surveys were performed with different source-receiver offsets (1.5, 3.0, and 6 m), and reverse shot gathers were acquired as well. Three to five shots were collected at each source location and seismic traces were vertically stacked to suppress the incoherent nose recorded by the array. Generally, surface waves were identified on the seismic profiles by their relatively lower velocities and dispersive characteristics. The geophone arrays were positioned across the center of the buried culvert (between channels 10 and 11). For the reverse shot gathers, the geophones remained in place while the energy source was positioned on the opposite end of the array, with the same source-receiver offsets.

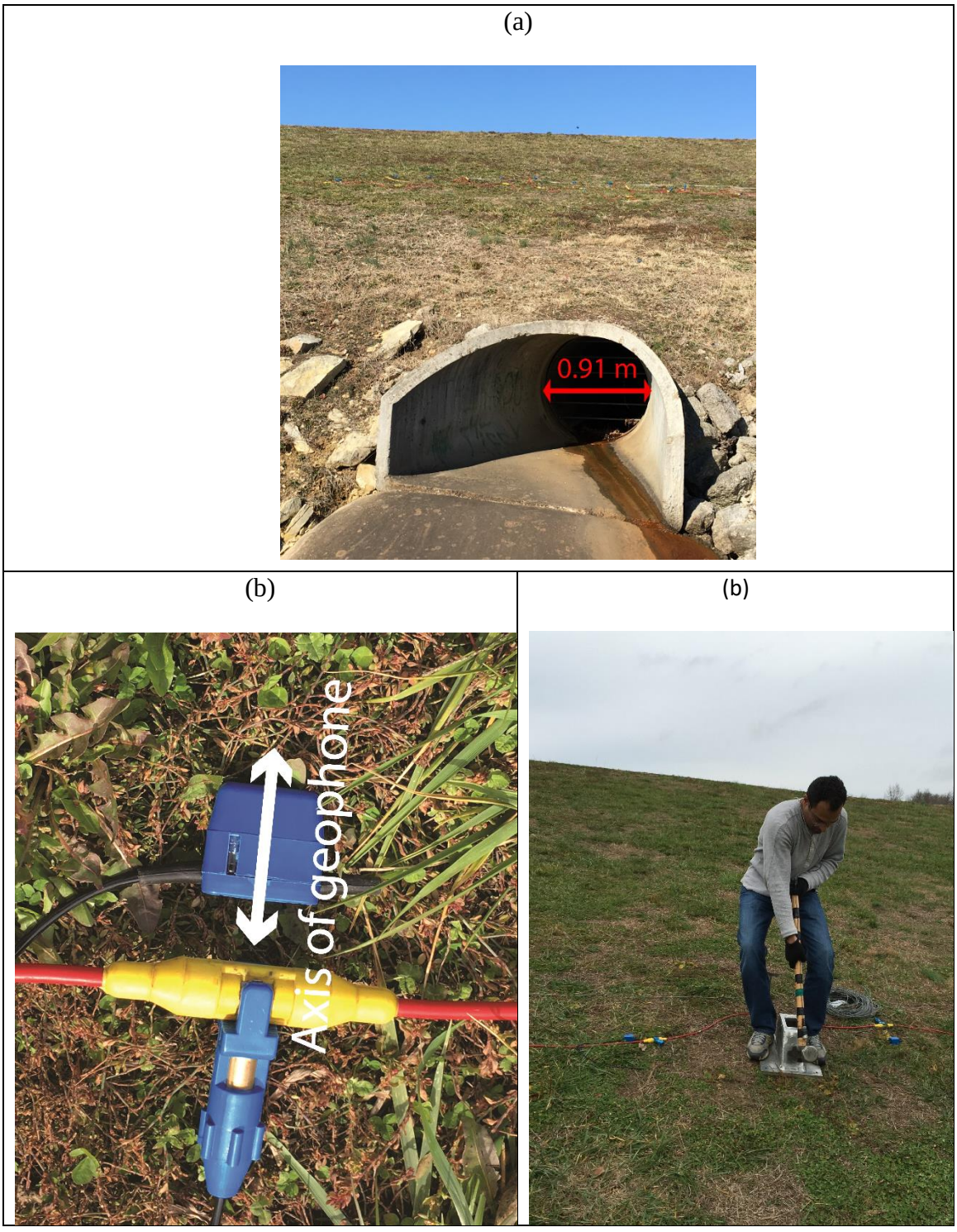

Figure 2.1. (a) Downstream outlet of the concrete conduit lying beneath an embankment dam. (b) Horizontal geophone. (c) Application of shear energy source.

The same set of experiments were carried out with vertical geophones (14 Hz and 100 Hz). The geometry of the surveys for the14 Hz vertical geophones were held constant for the 14 Hz horizontal geophones. However, for the 100 Hz vertical geophones, 24 geophone stations with spacings of 30 cm were employed.

In addition, the distance from the array to the top of the culvert decreased to 1.5 m for the 100 Hz vertical geophones. The reason for analyzing the shallower embedment depth was because the fundamental modes of the surface waves could be obtained later, during the processing step. Given that the wavelength is directly related to the reciprocal of the frequency. For the higher frequency geophones (100 Hz), the shorter distance of 1.5 m was considered, and the geophone array was positioned beneath channel number 6.

Following data acquisition, the seismic data were processed in the lab. The AARW technique (Nasseri-Moghaddam et al., 2005a; Putnam et al., 2009) was applied to study the attenuation characteristics of Rayleigh and Love waves. Before applying the AARW technique, an f-k filter was applied on the shot gathers to remove the direct P-waves, refracted waves, reflection, and air waves. The reason for remove the signals other than the surface waves is that the surfaces waves attenuate faster than body waves at large offsets. Therefore, to increase the S/N ratio, the f-k filter was applied. The f-k filter is a two dimensional Fourier transform from time-space domain to frequency-wavenumber domain. In the f-k domain, seismic events and noises can be more easily recognized and therefore be filtered out before an inverse Fourier transform is applied.

To perform the AARW technique (Nasseri-Moghaddam et al., 2005a; Putnam et al., 2009), a Discrete Fourier Transform (DFT) was performed on the time series (shot gathers), and the frequency amplitudes of the signals were thereby acquired. Then the

Normalized Energy-Distance (NED) parameters were calculated for each channel, according to Putnam et al. (2009):

$$NED_i = E_i \Big/ max(E_i) \tag{1}$$

where E_i is the cumulative signal energy at geophone station i. E_i, is the summation of the amplitude squared of all the frequency components for each geophone station:

$$\mathrm{E_i} = \sum_1^{\mathrm{N}} |\mathrm{A_f}|^2 \tag{2}$$

where A_f is the amplitude of the frequency component f, and the frequency spectrum is combined of *N* frequency components. According to Eq. 1, the cumulative energy was normalized to the maximum energy recorded across the geophone stations. A gain function was considered to compensate for the geometrical damping (Nasseri-Moghaddam et al., 2005a; Putnam et al., 2009). These processing steps were applied to both Love wave and Rayleigh wave seismic data sets.

As a final step, a phase shift analysis was carried out on the 100 Hz vertical geophone data sets to analyze the changes in the time lapse that would be expected to occur due to the presence of subsurface voids. Accordingly, the phase information was extracted from the frequency domain. Then, the phase shifts were unwrapped and plotted as function of frequency. The changes in the phase shift versus frequency indicates the time delay in signals.

3. RESULTS

First, the results were plotted for the vertical and horizontal 14 Hz geophones (Figure 3.1). Figure 3.1.a shows the Normalized Energy Density (NED) plot for a 20 channel system where Love waves were recorded. The source-receiver offset was 3 m to the right of the last geophone station (station number 20). Figure 3.1.a clearly illustrates the attenuation of the Love waves where a subsurface tunnel is present. The locations of the near and far boundaries of the conduit are shown by arrows. Although the Love wave energy decreased with increasing the distance from the source location, a very obvious "bump" in the energy can be seen (Figure 3.1.a), beginning in front of the near boundary of the conduit. Channels 12 and 11 (the energy is coming from the right side of the profile) indicate an increment in the Love wave energy, followed by a decline in the Love wave energy. The decrease in the energy of the Love waves lessens as the distance increases (Figure 3.1.a).

The same trend can be observed for the recorded energy of the Rayleigh waves, shown in Figure 3.1.b. The NED values represent the shear wave component of the Rayleigh waves. However, the highest energy of the Rayleigh waves was recorded in front of the near boundary of the buried conduit. The decrease in the energy of the Rayleigh waves appeared to be faster than the Love waves (Figure 3.1b vs. 3.1a). It is notable in Figure 3.1 that the initial decrease in the recorded energy of the Rayleigh waves (decrease in energy before the wave reached the near boundary of the conduit) first declined on channel 15, whereas for the Love waves, the decrease began at channel 13.

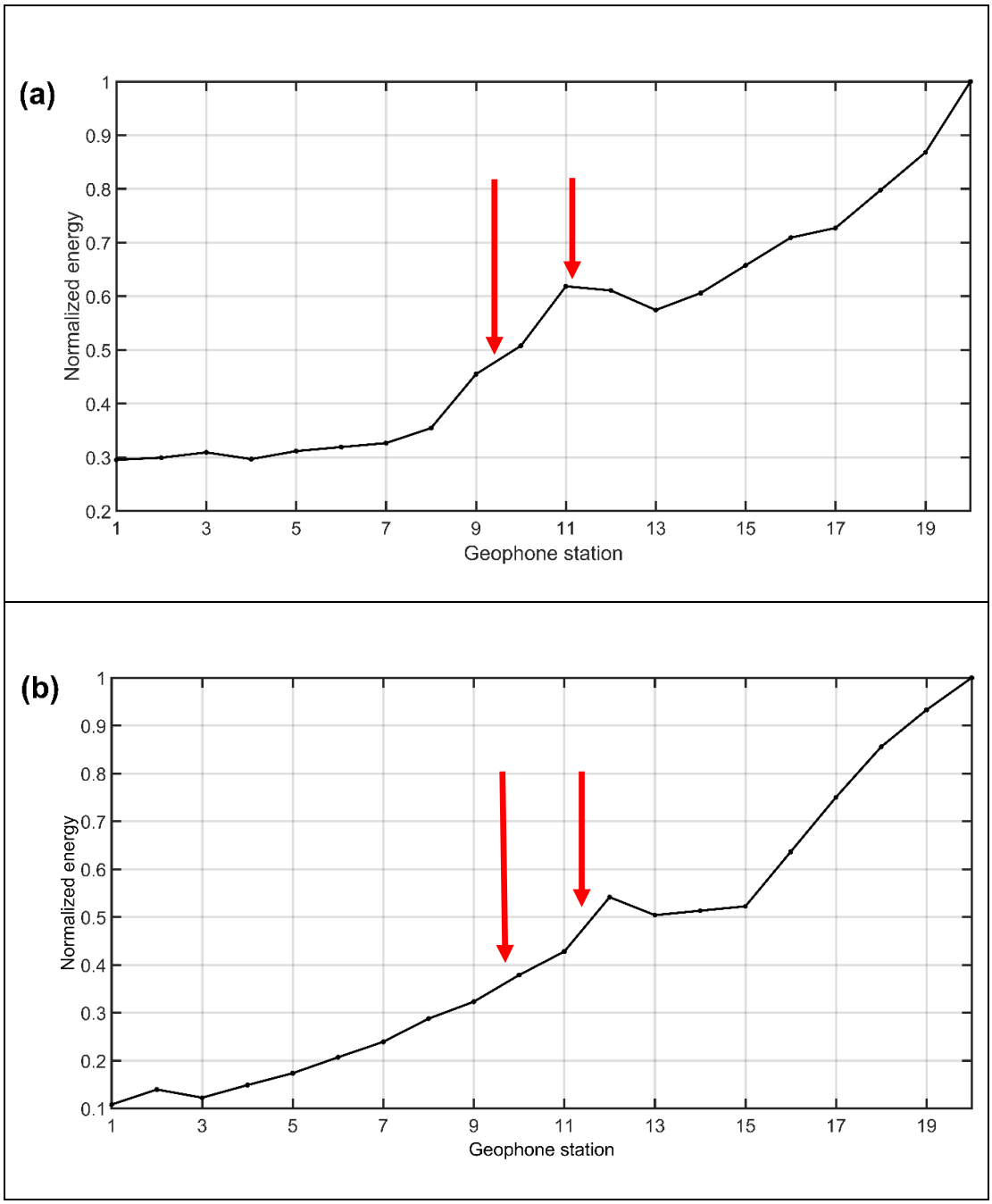

Figure 3.1 Normalized Energy Density (NED) plots for the embankment dam surveys over a reinforced concrete culvert, with a depth of embedment of 3.8 m. (a) 14 Hz horizontal geophones (Love waves). (b) 14 Hz vertical geophones (vertical components of Rayleigh waves). The red arrows show the buried conduit boundaries.

Figure 3.2 shows the NED analysis for the vertical 100 Hz geophone array. The energies represent the shear wave components of the Rayleigh waves. Note that in this survey the conduit embedment depth was 1.5 m. The source was located 1.5 m to the west of the first station. The plot in Figure 3.2 also shows that the peak for the NED occurs just in front of the near boundary of the conduit on channel 5 (the wave is propagating from west to east). Some small ripples in the calculated NEDs can be seen between channels 13 to 17 (Figure 3.2).

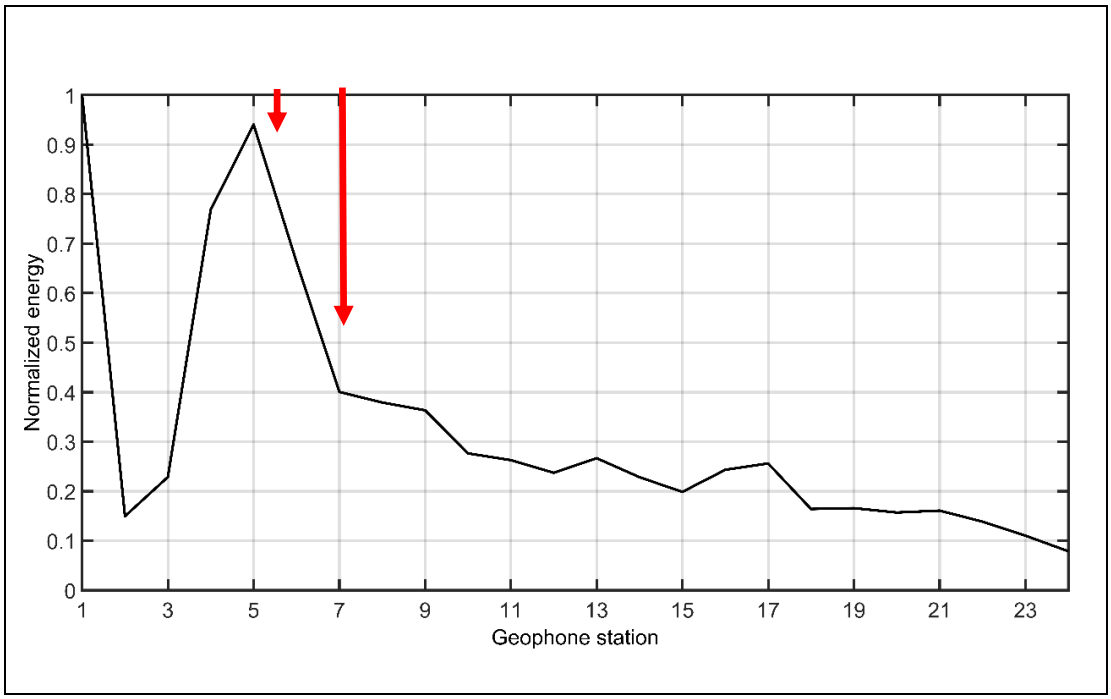

Figure 3.2. Normalized Energy Density plots for the reinforced concrete culvert with a depth of embedment of 1.5 m. Twenty four vertical 100 Hz geophones were used (recording vertical components of Rayleigh waves).

Figure 3.3 shows the power spectra (frequency amplitude squared for each frequency spectrum) for stations 1 and 20 of the 100 Hz geophones. This plot indicates how each frequency attenuated for the first station, compared to channel 20. It can be

seen that the higher frequencies attenuate more than the lower frequencies. In addition, the power spectra indicate that the highest frequencies generated and recorded in this experiment were in the range of 40 Hz to 70 Hz (or that is what the 100 Hz geophones recorded for this experiment). Figure 3.3 shows two spikes in the power spectra of the 85 and 105 Hz frequencies for station 1 which are absent at station 20.

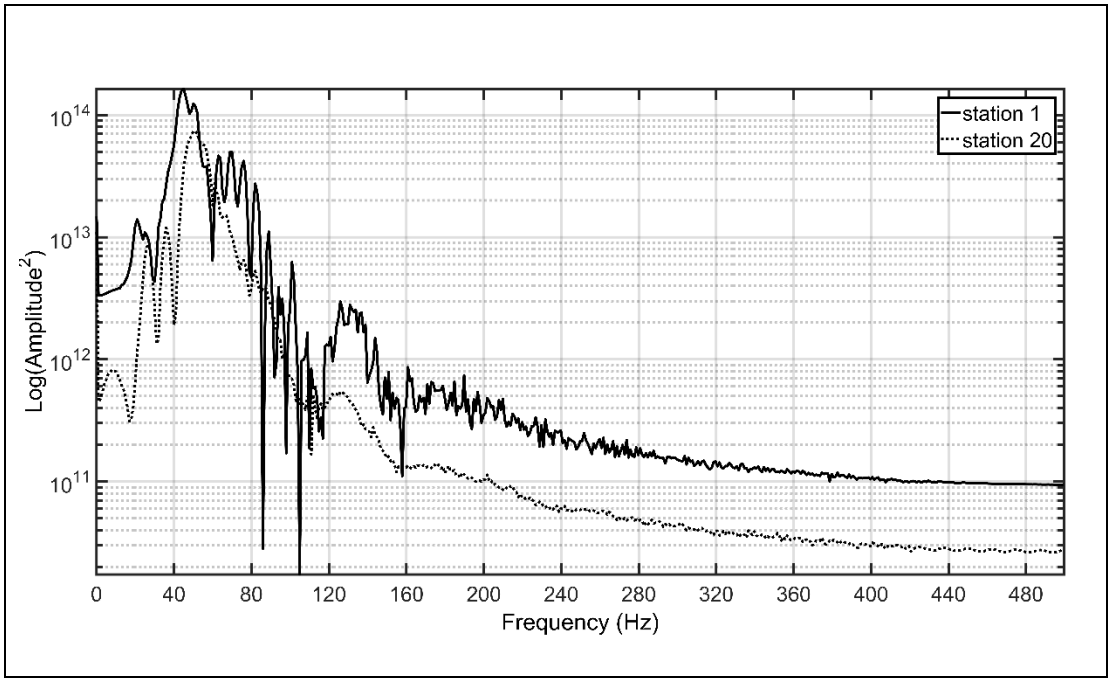

Figure 3.3. Power spectrum at stations 1 and 20 for the vertical 100 Hz geophones survey. Note how the surface wave energy dropped from station 1 to 20. The higher frequencies dropped greater than the lower frequencies. The energy is in logarithmic scale.

Finally, phase shift spectra were calculated as a function of frequency (Figure 3.4). The phase shifts for channels 1 to 24 are shown in different colors. The negative of the changes in the slope of the phase shift with respect to the frequency is termed the "time delay." Figure 3.4 shows the time delays for the arrival of the shear wave

component of the Rayleigh waves. It can be appreciated that the slopes of each channel changed very slowly, but constantly, indicating the arrival time of the Rayleigh waves for each station. However, channels 5 and 6 recorded anomalies in the slope of the phase shifts ranging from 100 Hz to 150 Hz, showing a larger time-lapse for the channel 6 (greater changes in the dip for the phase shift between those frequencies at channel 6). Channels 5 and 6 are indicated in bold red color for better tracking the described phase shifts. Above frequencies of 150 Hz, it can be seen that the frequencies were healed and the slopes of the phase shifts are more or less equal for channels 5 and 6. Moreover, the phase shift of channel 7 (bolded and in cyan color) can be seen intercepting channel 6 at 160 Hz with less dip. The turning points for the phase shift in channel 6 appeared to occur between 160 Hz and 210 Hz (wave healing).

No phase shift spectrums were plotted for the 14 Hz surveys. In fact, the total recording time for those two set of experiments (horizontal and vertical 14 Hz geophones surveys) was 0.5 s, whereas the recording time for the 100 Hz experiment was 1 s. Therefore, the resolution of the frequency spectrum (number of frequency points in 1 cycle) for the 14 Hz experiments were too low to allow for unwrapping. MATLAB unwraps the phase spectrum for jumps of equal to or greater than π for the consecutive elements in frequency domain, and adds multiples of 2π. The resolution in the frequency relates to the total recording time, and the highest frequency that can be resolved (Nyquist frequency) in the frequency domain, which is related to the time sample rate in the time domain. Even zero-padding techniques were unsuccessful in improving the frequency resolution. Therefore, no phase shift analysis was performed between the 100 Hz and 14 Hz frequencies.

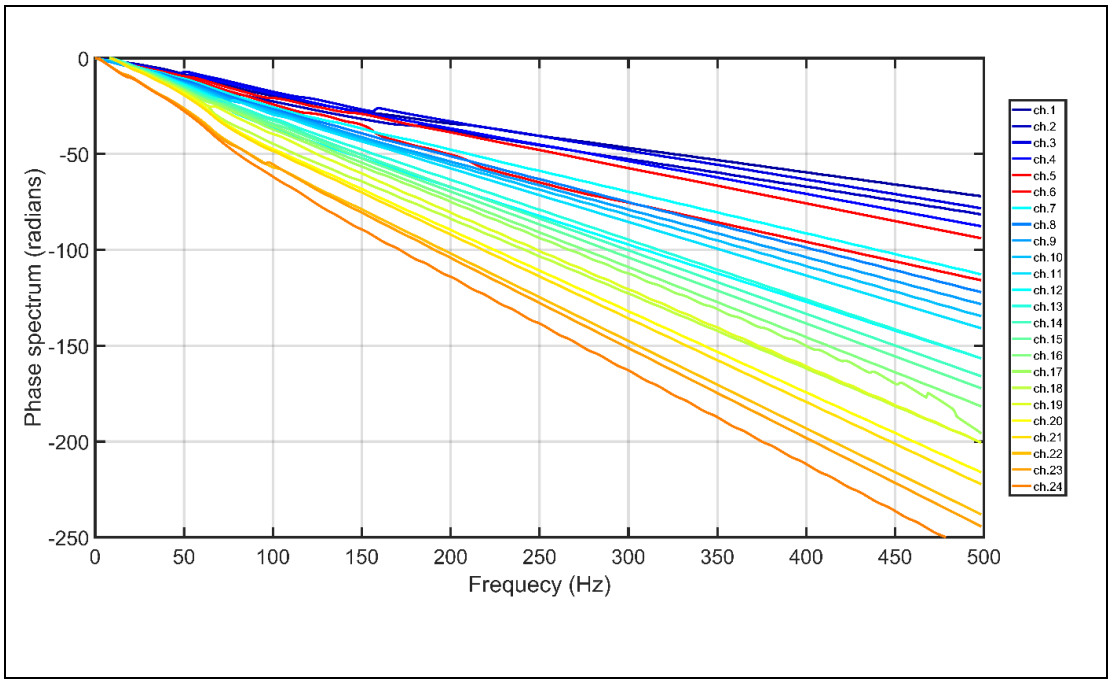

Figure 3.4. Unwrapped phase spectrum for the 100 Hz geophones survey over the embankment dam with 3 m of embedment depth.

4. DISCUSSION

First of all, since the energies were normalized with respect to the highest energy recorded across the channels (Figure 3.1 and 3.2), it cannot be deduced which type of surface waves carried a larger amount of energy (Love waves or Rayleigh waves). In the data acquisition we tried to reproduce the same amount of energy by discharging the source in a consistent manner for both experiments, by controlling the impact force on the shear source (Love waves) and the regular source (Rayleigh waves). However, generating a high impact source shot for the Love waves is challenging due to the nature of the shear source.

Figures 3.1 and 3.2 show the peak energy being recorded in front of the near boundary of the conduit tunnel, which is consistent with previous results (Nasseri-Moghaddam et al., 2005a; Nasseri-Moghaddam et al., 2007; Nasseri-Moghaddam et al., 2005b; Putnam et al., 2009). These energy peaks likely occurred due to the reflection of the seismic energy from the interface of different media (soil or concrete versus air-filled void). These results suggest that even for circular tunnels, the reflection of the seismic waves were observed. However, these reflections appear to be on the near boundary side of the conduit tunnel.

The Love wave experiments (Figure 3.1.a) exhibit a slightly more pronounced anomaly in the NED values than the Rayleigh waves (Figure 3.1.b) for the 14 Hz experiments. In the case of the 100 Hz experiment the anomaly is very obvious (Figure 3.2). In the 100 Hz experiments, the sources were intentionally set closer to the first receivers (1.5 m), because the higher frequencies generally attenuate faster than lower frequencies. One reason that the peak of the energy for the NED is more pronounced (on

Figure 3.2) than the energy peaks on either Figure 3.1.a or 3.1b is that the embedment depth of the conduit for the 100 Hz geophones surveys was shallower (1.5 m) than the other two surveys (3.8 m).

Figures 3.1 and 3.2 suggest that the energy attenuation in Rayleigh waves are slightly greater than the Love waves. However, the rate of loss in energy for the vertical 100 Hz geophones compared to vertical 14 Hz geophones appear to be more or less equal.

Figure 3.3 shows the power spectra for stations 1 and 20 in the 100 Hz experiment. Generally, higher frequencies attenuate with a higher rate than the lower frequencies. Figure 3.3 confirms the latter argument. The large amount of noise on the power spectra plot (Figure 3.3) is probably due to the bouncing of the sledge hammer after the first strike on the source plate (data acquisition issue). It is obvious that these spikes are of high frequencies (85 Hz and 105 Hz) and are absent at station 20. These types of noise are attenuated rather quickly.

Figure 3.4 shows the phase shift analysis for the 100 Hz experiment. Because surface waves are dispersive, different wavelengths (frequencies) penetrate to different depths in the subsurface. Therefore, not all the frequencies get disturbed by the presence of the air-filled voids (Park et al., 1998). The results summarized in Figure 3.4 indicate that the air-filled conduit causes a delay in arrival time of certain frequencies (frequencies 100 to 150 Hz).

Surface waves cannot propagate, theoretically, within the air-filled voids. The shear modulus of the air and water is zero and, therefore, the Love waves and the shear wave component of the Rayleigh waves cannot propagate in air-filled or water-

filled voids. Consequently, it could be expected that a time delay would occur in the vicinity of subsurface voids. Figure 3.4 shows such a time delay in the precise location of the buried conduit. On the other hand, those wavelengths that are much greater or much shorter than the size and depth of the conduit were not affected by the presence of the conduit tunnel. That is why “wave healing” can be observed on both sides of the anomaly ranges (waves are healed outside the range of 100 Hz to 150 Hz).

It is important to mention that zero-padding the time series for the 14 Hz experiments did not help improving the frequency resolution. The zero-padding technique is useful when the zeros are added to the time series where the amplitude values in time are already close to zero. In other words, the whole surface energy trend has been recorded completely at the channel.

5. CONCLUSIONS

In this study, three sets of seismic experiments were carried out over a buried conduit to evaluate the attenuation analysis of both Love waves and Rayleigh waves. The results of this study successfully identified the location of the buried conduit, at depths of up to 3.8 m. The attenuation analyses of the Rayleigh waves with the higher frequency geophones (100 Hz) indicated more pronounced anomalies in the NED values. Anomalies were also observed in the phase shift spectra of the 100 Hz experiments. However, the phase shift study for the 100 Hz experiments revealed only subtle anomalies. In a previous study by Hajiani et al. (currently in review), the authors successfully demonstrated that the time delay analysis is a powerful technique to detect shallow underground tunnels (up to 3.8 m depth). However, in this study, the time delay analysis of the high frequency geophones showed that high frequencies are less affected by the presence of subsurface tunnels. However, if the embedment depths of the voids are much less than 1.5 m, or the size of the tunnels are larger than 0.9 m, then greater anomalies could be expected to in the phase shift spectra, even with the higher frequency geophones.

Further studies need to be performed to evaluate the sensitivities of the new proposed techniques. Numerical studies are suggested for the evaluation of the time-lapse analysis of the surface waves. In addition, an empirical relation between the affected frequencies in the phase spectrum domain should be established with the sizes and/or embedment depths of the tunnels.

ACKNOWLEDGMENTS

The authors would like to appreciate the Exploration Geophysics Lab of the Missouri University of Science and Technology for providing with the seismic equipment and helping in data acquisition.

REFERENCES

Engelsfeld, T., Šumanovac, F., Pavin, N., 2008. Investigation of underground cavities in a two-layer model using the refraction seismic method. Near Surface Geophysics 6, 221-231.

Frehner, M., Schmalholz, S.M., Saenger, E.H., Steeb, H., 2008. Comparison of finite difference and finite element methods for simulating two-dimensional scattering of elastic waves. Physics of the Earth and Planetary Interiors 171, 112-121.

Gelis, C., Leparoux, D., Virieux, J., Bitri, A., Operto, S., Grandjean, G., 2005. Numerical modeling of surface waves over shallow cavities. Journal of Environmental and Engineering Geophysics 10, 111-121.

Grandjean, G., Leparoux, D., 2004. The potential of seismic methods for detecting cavities and buried objects: Experimentation at a test site. Journal of Applied Geophysics 56, 93-106.

Hajiani, P., Anderson, N.L., Rogers, J.D., currently in review. Phase Shift Analysis of Surface Waves to Detect Underground Openings. NDT & E International.

Herman, G.C., Milligan, P.A., Huggins, R.J., Rector, J.W., 2000. Imaging shallow objects and heterogeneities with scattered guided waves. Geophysics 65, 247-252.

Nasseri-Moghaddam, A., Cascante, G., Hutchinson, J., 2005a. A new quantitative procedure to determine the location and embedment depth of a void using surface waves. Journal of Environmental and Engineering Geophysics 10, 51-64.

Nasseri-Moghaddam, A., Cascante, G., Phillips, C., Hutchinson, D.J., 2007. Effects of underground cavities on Rayleigh waves-Field and numerical experiments. Soil Dynamics and Earthquake Engineering 27, 300-313.

Nasseri-Moghaddam, A., Phillips, C., Cascante, G., Hutchinson, D.J., 2005b. Detection of underground cavites using MASW test, 33rd CSCE Annual Conference 2005, Toronto, ON, pp. GC-270-271-GC-270-211.

Nolan, J.J., Sloan, S.D., Broadfoot, S.W., McKenna, J.R., Metheny, O.M., 2011. Near-surface void identification using MASW and refraction tomography techniques, SEG Technical Program Expanded Abstracts, pp. 1401-1405.

Park, C.B., Miller, R.D., Xia, J., 1999. Multichannel analysis of surface waves. Geophysics 64, 800-808.

Park, C.B., Xia, J., Miller, R.D., 1998. Ground roll as a tool to image near-surface anomaly. 68th Ann. Internat. Mtg., Soc. Expl. Geophys., 874-877.

Putnam, N.H., Peng, X., Cawlfield, J.D., Kovin, O.N., Torgashov, E.V., Modur, P., Stagner, C., Grant, S.L., Anderson, N.L., Nasseri-Moghaddam, A., 2009. Attenuation analysis of Rayleigh waves used to locate shallow manmade tunnels, 43rd U.S. Rock Mechanics Symposium and 4th U.S.-Canada Rock Mechanics Symposium, Asheville, NC.

Xia, J., Miller, R.D., Park, C.B., 1999. Estimation of near-surface shear-wave velocity by inversion of Rayleigh waves. Geophysics 64, 691-700.

Xia, J., Nyquist, J.E., Xu, Y., Roth, M.J.S., Miller, R.D., 2007. Feasibility of detecting near-surface feature with Rayleigh-wave diffraction. Journal of Applied Geophysics 62, 244-253.

Xia, J., Xu, Y., Luo, Y., Miller, R.D., Cakir, R., Zeng, C., 2012. Advantages of Using Multichannel Analysis of Love Waves (MALW) to Estimate Near-Surface Shear-Wave Velocity. Surv. Geophys. 33, 841-860.

Xia, J., Xu, Y., Miller, R.D., Nyquist, J.E., 2006. Rayleigh-wave diffractions due to a void in the layered half space, SEG Technical Program Expanded Abstracts, pp. 1406-1410.

Zeng, C., Xia, J., Miller, R.D., Tsoflias, G.P., 2009. Modeling results on detectability of shallow tunnels using rayleigh-wave diffraction, SEG Technical Program Expanded Abstracts, pp. 1425-1429.

III. IDENTIFYING SUBSURFACE STRATIGRAPHY USING DISPERSIVE CHARACTERISTICS OF GPR DATA

Payman Hajiani [a*], Katherine R. Grote [a], Andrew Parsekian [b]

[a] Department of Geosciences and Geological and Petroleum Engineering, Missouri University of Science and Technology, Rolla, MO 65409, USA

[b] Department of Geology and Geophysics, University of Wyoming, Laramie, WY 82071, USA

ABSTRACT

Dispersive Ground Penetrating Radar (GPR) signals can occur when a thin surficial layer overlies a basal layer of much greater or much smaller dielectric permittivity, such as a layer of ice overlying liquid water or a saturated zone overlying relatively dry soil. Dispersive signals can be analyzed using inversion of the phase velocity vs. frequency curve and can be used to estimate the permittivity and thickness of the overlying soil layer. Most studies of dispersive GPR waves have used either modeled simulations or data acquired under natural, non-controlled conditions, where layer heterogeneity can make evaluating the accuracy of this technique difficult. In this research, we evaluate the formation of dispersive waves within a large experimental tank where the permittivity and thickness of each soil layer is controlled. Within this tank, a basal soil layer was created, and variable-offset GPR data were acquired across this layer using four frequencies (100-, 250-, 500-, and 1000-MHz). Thin (3-cm) layers of soil with a contrasting permittivity were then placed over the basal layer, and GPR data acquisition was repeated after the addition of each layer, until the thickness of the overlying layer

was 54 cm. The experiment was performed six times; three experiments had saturated sand, silt, or organic soil as the basal layer and dry layers of the same soil type as the overlying layer. The other three experiments used dry soil as the basal layer and saturated soil for the overlying layers. Data analysis showed that in most cases, thickness and permittivity estimates from dispersive signals were more accurate when intermediate frequencies (250- and 500 MHz) were employed. The accuracy of results is strongly influenced by the permittivity of the overlying layer, where drier overlying layers were better characterized by dispersive wave analysis than wetter overlying layers, which probably acted as leaky waveguides.

1. INTRODUCTION

Guided wave analysis of thin layer is useful in a variety of contexts. Researchers have used guided waves to estimate the thickness and saturation of wet soil layer overlying drier soil [1, 2] and to estimate the thickness of ice over water [3, 4]. Similarly, guided wave technology has applications in understanding how irrigation moves through an agricultural soil or in measuring ice or permafrost thickness [5], which is important for understanding the effects climate change in the Arctic and Antarctic.

Guided waves do not occur in all thin layers near the ground surface. The formation of guided waves depends on the thickness of the thin layer [6], the moisture content of the overlying layers and the geologic materials below [4, 5, 7], the dielectric constants of the thin layer and the underlying layer [8]. Until now, according to the best of the authors knowledge, no unique research study has been performed to analyze the effects of the GPR antenna frequencies to identify the geologic thin layers. This study presents the results of a comprehensive set of experiments in which four different GPR antenna frequencies (100-, 250-, 500-, and 1000-MHz) have been employed to identify the permittivity and thickness of geologic thin layers.

Guided waves also need adequate distance between the transmitting and receiving antenna to allow resonance to occur [8]. These conditions have made it difficult to test guided wave theory in the laboratory, so the accuracy of the computational code that estimates guided layer properties is unknown.

Although, many research studies [1, 3-5] have been performed to analyze the GPR signals in identifying the thickness and permittivity of thin layers, no laboratory study was performed with controlled environment. For instance, van der Kruk et al. [6]

studied the dispersive GPR data to determine the properties of precipitation-induced multilayer surface waveguides. However, in order to verify their results, a trench had been excavated 100 m away from the survey location and the soil properties such as resistivity and other soil properties. In other words, no evidence was available to confirm that the subsurface materials under the survey location were homogeneous. Another study by Arcone et al. [1] used GPR reflection profiles, a trench, and a well log to determine the physical properties of their experimental site. In the other study by Arcone [3], only the median thickness of the overlying ice cover has been reported for their Birch Lake study. However, for the other site location in that study [3], available drill holes allowed the verification of subsurface jointing and presence of groundwater.

Therefore, in this study a set of laboratory experiments were carried out with a controlled soil environment. A large (4m x 3m x 1.2m) fiberglass tank were made and three different soil types (sands, organics, and silts) were used. For each soil type, overlying layers of soil with a great contrast moisture content with respect to the basal layer were added, 3 cm at a time, so that the thickness and permittivity estimations of the computational method can be studies for a controlled environment. Four different GPR antennas (100- , 250-, 500-, and 1000- MHz) were employed to acquire ground penetrating radar data sets. and the frequency of the GPR antenna. In this study, the effects of the antenna frequencies on the dispersion characteristics of the subsurface thin layers with contrasting primitives were studied. The results of this project confirmed that intermediate frequencies (250- and 500-MHz) resolve the thin layer parameters better, at least for the experimental set-ups in this project.

The main purpose of this research is to investigate the accuracy of computational model that analyze the frequency and arrival times of ground penetrating radar (GPR) guided wave data to determine the thickness and dielectric permittivity of thin subsurface layers. The currently used computational model has never been tested in a controlled environment, as the conditions necessary for guided waves to occur are difficult to produce at the laboratory scale. Some researchers [9] have developed a MATLAB code that analyzes GPR data to determine whether guided waves are present in the data set, and if those guided waves are present, to estimate the thickness and dielectric permittivity of the thin layers. Here in this study, a unique laboratory experiments were perfumed to investigate the functionality of that computational model and to resolve physical properties of thin subsurface layers.

Guided waves may occur when a thin layer near the ground surface has a permittivity that is very different from that of the underlying material (Figure 1.1). When these conditions occur, the thin layer can trap and internally reflect the electromagnetic waves emitted from the GPR transmitter, resulting in dispersive wave propagation. These waves are known as “guided waves”, and their occurrence can cause conventional methods of GPR data analysis to fail [9]. According to Bilowski et al. [10], electromagnetic waves may trap in these thin layers when the thickness of these layers are relatively equal or smaller than the GPR wavelength of the GPR signal. In the event that the electromagnetic waves are trapped in these thin layers, waveguides form (Figure 1.1).

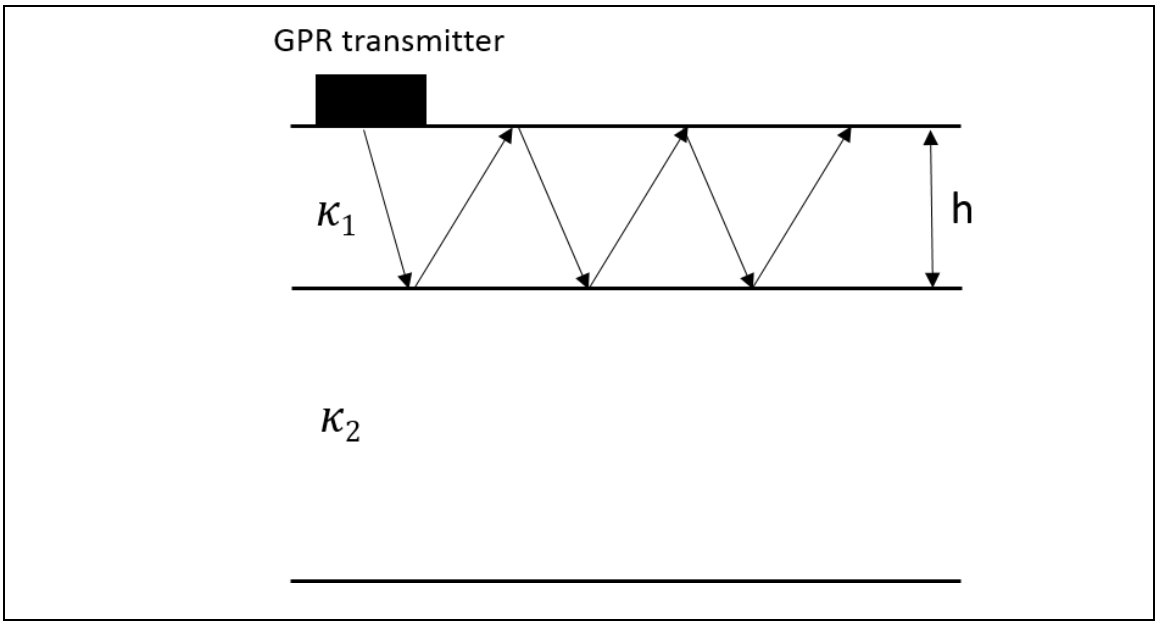

Figure 1.1. Guided waves are trapped within a thin surficial layer of thickness h when the overlying and underlying layers have very different dielectric permittivities (κ_1 and κ_2).

Transverse electric (TE) fields occur when electric field pattern of radiation is perpendicular to the propagation direction of the electric waves. Transverse modes occur in radio waves and microwaves confined to a waveguide.

Due to the constraints of the boundary conditions, there are only limited frequencies and forms of the wave function which can propagate in the waveguide. The lowest frequency in which a certain mode can propagate is the cutoff frequency of that mode. The mode with the lowest cutoff frequency is the fundamental mode of the waveguide and its cutoff frequency is a function of the waveguide thickness [1, 7, 8, 11].

According to Arcone [3], "the group velocity for the GPR signals is the propagation velocity for energy at any particular frequency and is found by [12]":

$$v_{gr} = v_{ph}/(1 - \frac{f}{v_{ph}}\frac{dv_{ph}}{df}), \quad (1)$$

where *f* is the frequency, v_{ph} is the phase velocity, and v_{gr} is the group velocity.

Dispersion curves shows the changes of phase velocity with respect to frequency components of the wave. The dispersion curves can be calculated based on a computational technique developed in previous studies [13].

The data acquisition and processing methods were described in details in the next section. Then, the results of the study were shown so that the readers should be able to develop their explanations about the results without influenced by the author's opinions. Next to the result section, the discussion has been provided based on the results of this study and conclusions were drawn finally.

2. DATA ACQUISITION

This project investigated guided wave formation as a function of layer thickness, dielectric permittivity, GPR frequency, and soil texture. In this project, three soil textures (sand, organic soil, and silt) were investigated, and guided wave formation was examined using dry and wet conditions for each soil texture, for a total of six experiments. All experiments were performed within a 3.7 m x 2.4 m x 1.2 m experimental tank (Figure 2.1) that was constructed from high strength fiberglass and without any metal components, as metal might influence the GPR wave propagation. For each soil type, layers with carefully controlled water contents were used to create an environment in which guided waves might develop. All experiments had a basal layer of either very wet or very dry soil, and the thickness of this basal layer remained constant throughout the experiment. Over this basal layer, an overlying layer of contrasting soil moisture was installed. The overlying layer had an initial thickness of 3 cm, and the thickness of this layer was increased in 3 cm increments throughout the experiment, until the final depth of the overlying layer was greater than 50 cm. GPR surveys were acquired with four frequencies for each layer thickness (each time soil was added to the tank). For Experiment 1, a basal layer of homogenously saturated sand was placed in the tank, and thin layers of completely dry sand were incrementally placed on top of the basal layer. For Experiment 2, a basal layer of dry sand was overlain by incremental layers of saturated sand. For Experiment 3, a basal layer of saturated organic soil was overlain by incremental layers of dry organic soil, and Experiment 4 used a basal layer of dry organic soil overlain by saturated organic soil. Similarly, Experiment 5 had a saturated basal layer of silt with overlying dry silt layers, while Experiment 6 has a basal layer of dry silt

overlain by saturated silt layers. Section 4.1 describes the soil preparation for all experiments, Section 4.2 describes the placement of the soil in the tank, Section 4.3 describes GPR data acquisition, and Section 4.4 discusses the methods used to monitor the soil water content within the tank throughout all experiments.

Figure 2.1. The experimental tank was constructed with no metal and filled with flat layers of soil. In this figure, 250 MHz antennas are being moved over dry sand.

2.1. SOIL PREPARATION

The dielectric permittivity of soils is primarily controlled by soil water content. Thus, to create layers with uniform and distinct permittivities, the soil water content had

to be carefully controlled. To create soil layers with homogeneous water content, only very wet (at or near saturation) and very dry soil layers were used. To create dry soil for each experiment, the necessary volume for each soil type was dried in a large industrial oven for 24 hours at 110°C to ensure that all pore water was removed. As only a portion of the soil could be placed in the oven at one time, the dry soil was stored in air-tight drums until the entire volume had been dried. To prepare the saturated soil, the initial water content of the soil was determined, then known quantities of soil and water were placed in a mechanical mixer. As the soil was mixed, additional water was added as necessary until the soil had a uniform volumetric water content that was close to saturation. Several gravimetric water content and soil density measurements were acquired from the saturated soil each time the mixer was used to calculate the volumetric water content and to verify the homogeneity of the saturation. Saturated soil was also stored in air-tight drums until sufficient soil for each soil layer had been processed.

2.2. SOIL PLACEMENT

An appropriate volume of soil was added to the tank to create a layer of the desired thickness, and the soil was carefully leveled, first by hand, then by using a "sweep" to ensure constant thickness throughout the tank. GPR data were acquired after each addition of soil, as described in section 2.3. When the basal soil layer was saturated and the overlying layers were dry, a 0.4 mm plastic sheet was placed over the saturated basal layer and was secured to the sides of the tank to prevent water from escaping from this layer. Dry soil was then placed in layers upon the plastic sheet. When the basal soil layer was dry and the overlying layers were saturated, a 1.1 mm rubber liner was placed over the dry soil; a rubber liner was used for this experiment instead of a plastic sheet to

ensure that no leaks would occur into the dry basal layer. Preliminary studies showed that neither the plastic sheet nor the rubber liner used in these experiments affected electromagnetic wave transmission. The plastic sheet was easier to conform to the exact tank dimensions and was sufficient to prevent upward migration of water, but a thicker rubber liner was needed to prevent downwards drainage. Saturated soil layers were constructed on top of this rubber liner.

2.3. GPR DATA ACQUISITION PARAMETERS

GPR data were acquired using a pulseEKKO Pro system (Sensors and Software) with 100, 250, 500, and 1000 MHz antennas. After each layer of soil was placed in the tank and carefully leveled to the desired thickness, three variable-offset surveys (two wide angle reflection and refraction (WARR) surveys and one common-midpoint (CMP) survey) were acquired with each frequency. For the 250, 500, and 1000 MHz antennas, the transmitting and receiving antennas were initially placed in contact with each other, then were incrementally moved apart. A similar procedure was followed for the 100 MHz antennas, but the initial antenna offset was 100 cm. The spatial sampling intervals for the variable-offset surveys were 10 cm for the 100 MHz antennas, 2 cm for the 250 and 500 MHz antennas, and 1 cm for the 1000 MHz antennas. For the first WARR survey, the transmitter was placed 1 m from the northern end of the tank while the receiver was incrementally moved towards the south. The second WARR was similar, with the transmitter located 1 m from the southern end and the receiver moving incrementally to the north. For the CMP survey, both antennas were placed in the center of the tank and incrementally moved apart. To avoid soil compaction, no one entered the tank after the soil was added. Instead, the antennas were moved remotely (Figure 2.1).

2.4. MONITORING SOIL WATER CONTENT

To monitor the dielectric permittivity within the tank, time domain reflectometry (TDR) probes were installed around the perimeter of the tank within each layer of soil. The TDR probes were 7.5 cm long and were installed at six stations around the tank (two stations on each long side and one station at each shorter side, as shown by the collections of vertical cables in Figure 2.1. At each station, TDR probes were installed horizontally with a vertical spacing of 6 cm between probes. The depth of probe installation at different stations was staggered for adjacent layers of soil, so three TDR probes were installed in each 3 cm layer. TDR data were acquired at least once an hour using an automated TDR system with 14 multiplexers connected to a Campbell Scientific TDR100 reflectometer and datalogger. The number of TDR probes placed in the basal layer varied somewhat between experiments, depending on whether the basal layer was dry or saturated. For experiments when the basal layer was saturated, three probes were buried in the saturated basal layer for each TDR station. For experiments where the basal layer was dry, fewer probes were placed in the basal layer, because the permittivity of the dry soil was not expected to change with time and since the TDR cables were shown to serve as potential conduits for leaks during a pilot study of this configuration. The six probes placed in the dry basal layer were located 3 cm beneath the rubber liner separating the basal and overlying layers so that any leaks would be detected quickly.

In addition to the TDR probes installed around the tank perimeter, at least two gravimetric water content samples were collected near the middle of the tank for each layer of soil, both when the soil was being placed in the tank and after the experiments were completed and the soil was being excavated. These samples showed that the water

content did not change with different layers of soil and that the water content in the center of the tank did not change significantly during the experiment. Since permittivity is strongly dependent upon water content, the consistency of the gravimetric water content measurements helps to verify the uniformity of the permittivity in each layer throughout these experiments.

2.5. PROCESSING METHODS

In this research project, the collected GPR data were processed using the method developed by van der Kruk et al. [4, 8]. This technique is based on the method of imaging dispersion curves for Multichannel Analysis of Surface waves (MASW) developed by Park et al. [13]. The first step in this processing technique is to use the Fourier transform to change from the offset-time domain, into the offset-frequency domain:

$$\widehat{U}(x,f) = \int U(x,t)\, e^{-i2\pi f t} dt \qquad (2)$$

where $\widehat{U}(x,f)$ is the wave-field in the offset-frequency domain and $U(x,t)$ is the wave-field in the time-offset domain. Having the frequency components (amplitude and phase values) of the wave-field, $\widehat{U}(x,f)$ can be separated into multiplication of the phase and amplitude spectra. It is necessary to realize that the attenuation information is included in the amplitude term, and the phase term contain the information on arrival times [13]. The phase velocity for each frequency component [8] is then given by:

$$v = \frac{-i2\pi f \Delta x}{\Delta \phi}, \qquad (3)$$

where v is the phase velocity for each frequency component, $\Delta\phi$ is the change in phase, and Δx is the change in offset. Then, the function of the wave-field in the frequency-phase domain, $\widehat{W}(f,\varphi)$, was obtained by applying the following integral transformation to $\widehat{U}(x,f)$:

$$\widehat{W}(f,\varphi) = \int e^{i\varphi x} \frac{\widehat{U}(x,f)}{|\widehat{U}(x,f)|} dx = \int e^{-i(\phi-\varphi)x} \frac{\hat{A}(x,f)}{|\hat{A}(x,f)|} dx. \quad (4)$$

As discussed above, the wave-field function can be written as $\widehat{U}(x,f) = e^{i\phi x}\hat{A}(x,f)$, where $\hat{A}(x,f)$ is the amplitude term and $e^{i\phi x}$ is the phase spectrum term. Accordingly, maximums for $\widehat{W}(f,\varphi)$ were obtained as the following criteria was fulfilled in Eq. (3):

$$\varphi = \phi = 2\pi f/v. \quad (5)$$

Thus, , Eq. 4 needs to be fulfilled to derive the peaks for $\widehat{W}(f,\varphi)$. Therefore, the phase velocity for each frequency component was determined when the maximums for the wave-field in the frequency-phase domain were identified. Using this methodology, the dispersion curves (phase-velocity vs. frequency) were constructed for all the GPR data sets.

The next step in data processes was to estimate the physical properties, dielectric permittivity and guided wave layer thickness, using the inversion method of "minimizing the cost function" [8]. In this study, the MATLAB code developed by van der Kruk et al. [9] was used to extract the dispersion curves for the GPR data sets and to invert them for surface waveguide properties. The code was run for each GPR data set; over the course of six experiments and four GPR frequencies (100-, 250-, 500-, and 1000-MHz), this totaled approximately 500 analyses. For each analysis it was determined whether guided waves were present. Figure 2.2 displays a typical transverse electric (TE) GPR survey acquired with the CMP method. The dispersion characteristics of the GPR signals can be seen (Figure 2.2) as a "shingled" pattern that occurs at larger offsets. Also, it is seen clearly that the GPR signals dispersed with increasing offsets. Dispersion is observed as a lengthening of the energy packet with respect to time; at small offsets, the energy packet

occurs in a relatively small time window, while dispersion causes the energy packet to occur in a longer time window at longer offsets. These two criteria (shingling and dispersion) were used to identify whether or not the dispersive waveguides formed [9]. If guided waves occurred, the dispersion curves were obtained and were inverted for the thickness and permittivity of the overlying layer. It is important to note that the dispersive waves were not fully formed in all experiments and therefore, those experiments yielded high errors in thickness and permittivity estimates.

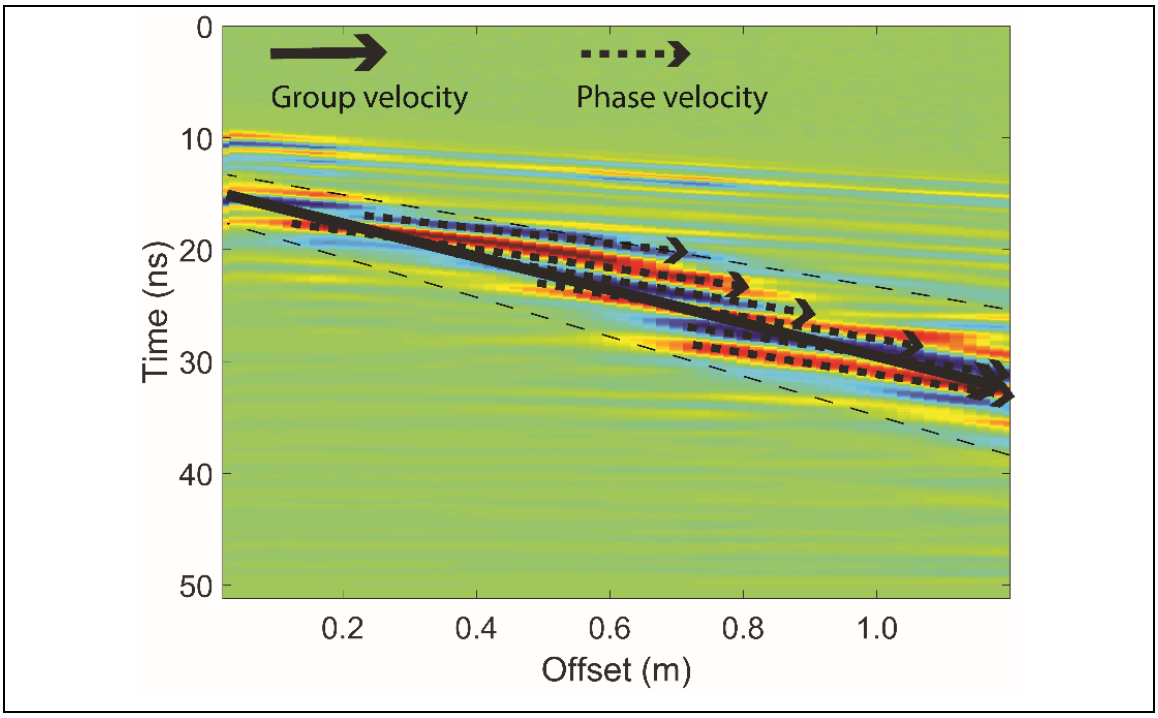

Figure 2.2. Measured GPR (500 MHz) data set for experiment 1 performed with CMP method. The overlying layer is dry sand with 3 cm thickness over 18 cm layer of basal saturated sand.

3. RESULTS

This section presents the results of this research project. First, CMP versus WARR surveys results are considered. Then, the quality of the data and error functions for the estimated thickness and permittivities will be remarked. The discussion of the results comes in the next session.

3.1. CMP AND WARR SURVEYS

Three variable offset surveys (two WARRS and one CMP) were acquired for each layer thickness in all experiments. To see if the method of data acquisition affected the results, both CMP and WARR data sets were processed for all layers in experiment 1. As will be discussed later, comparison of the results of CMP and WARR surveys indicated that the dispersion curves (Figure 3.1) and the inversion results (Table 3.1) did not depend on the method of data acquisition. The CMP and WARR trace-normalized surveys (Figure 3.1) reveal similar shingled reflections and similar dispersive guided waves. In addition, the dispersion curves of phase velocities indicated that fundamental and higher TE modes for both CMP and WARR gathers are identical (Figure 3.1). Therefore, data processing was performed only on CMP data sets for the rest of the experiments.

In addition to considering dispersive wave input data, inversion results for both CMP and WARR surveys were compared and were found to have very similar values. Table 3.1 summarizes the inversion results for both CMP and WARR data sets acquired with 500 MHz antenna. Error of inversion in Table 1 implies how well the inversion results fitted the measured parameters (known thickness and permittivity values ions).

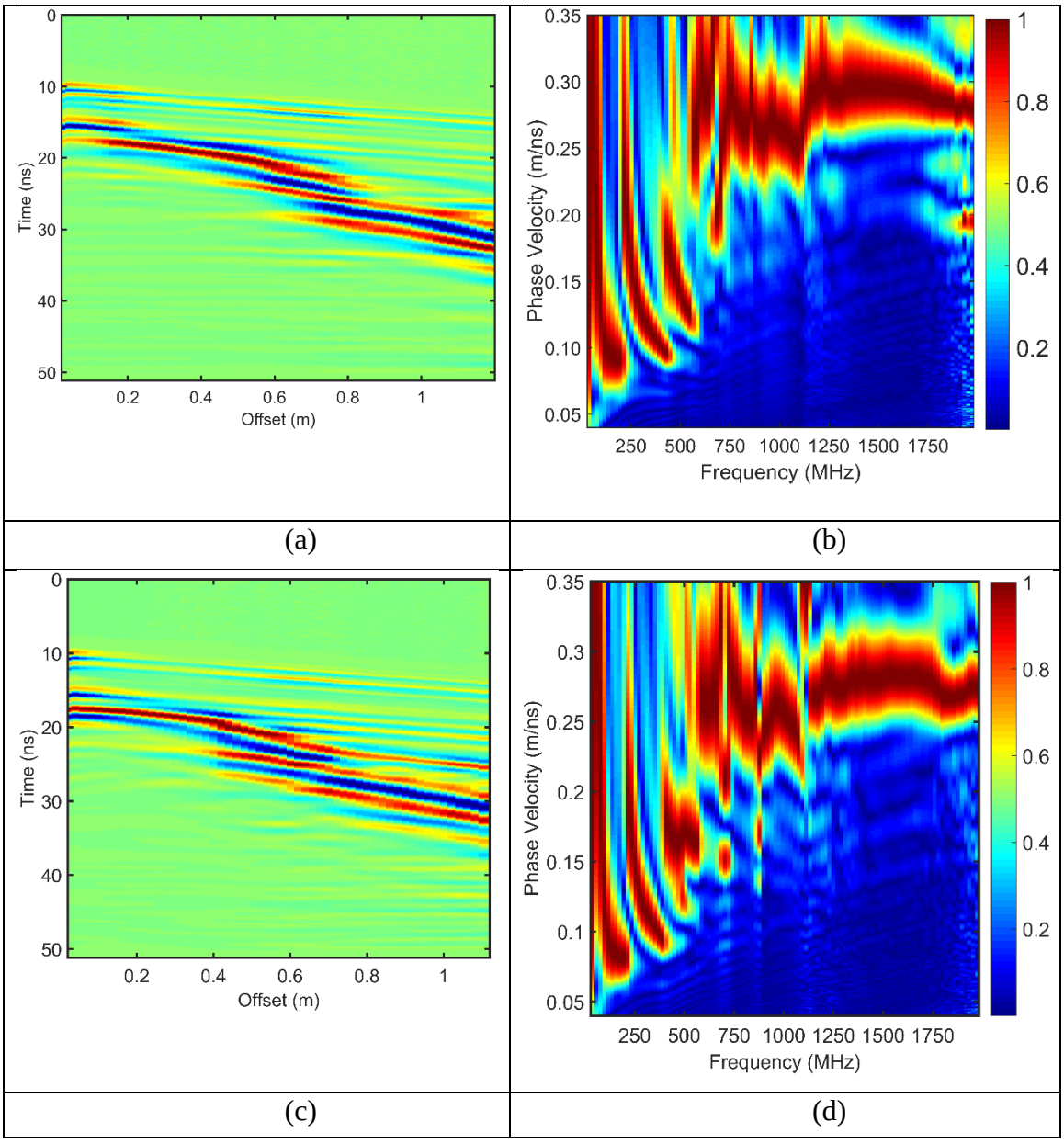

Figure 3.1. Processing results for experiment 1, surveys acquired with a 500 MHz antenna over 3 cm of dry sand overlying wet sand. (a) CMP and (c) WARR trace-normalized gathers. (b) CMP and (d) WARR phase-velocity spectra.

Table 3.1. Inversion Results for both CMP and WARR surveys (500 MHz frequency).

	Known layer thickness (cm)	Estimated Permittivity	Estimated Thickness (cm)	Error of the inversion
CMP	3	16.11	29	0.028
WARR	3	15.24	30	0.022
CMP	6	27.07	7	0.003
WARR	6	25.04	8	0.002
CMP	12	4.26	16	0.005
WARR	12	3.98	17	0.006
CMP	15	3.79	20	0.002
WARR	15	3.69	21	0.002
CMP	18	3.68	25	0.002
WARR	18	3.52	27	0.003

The similarity of results from WARR and CMP surveys validates the decision to process only one survey/layer for experiments 2 – 6. In Table 3.1, it should be noted that the thickness and permittivity estimates for the thinnest layers (3 and 6 cm of dry sand overlying wet sand) are very poor.

3.2. DATA QUALITY

During data processing, it became apparent that the quality of the dispersion images varied widely for different GPR frequencies. The worst dispersion images were obtained for 100 MHz data, while the 1000 MHz data also frequently had poor dispersion curves. The same pattern was observed for all the experiments regardless of the soil textures or the soil moisture content. Figure 3.2 shows typical poor dispersion images for 100 MHz and 1000 MHz in experiment 2.

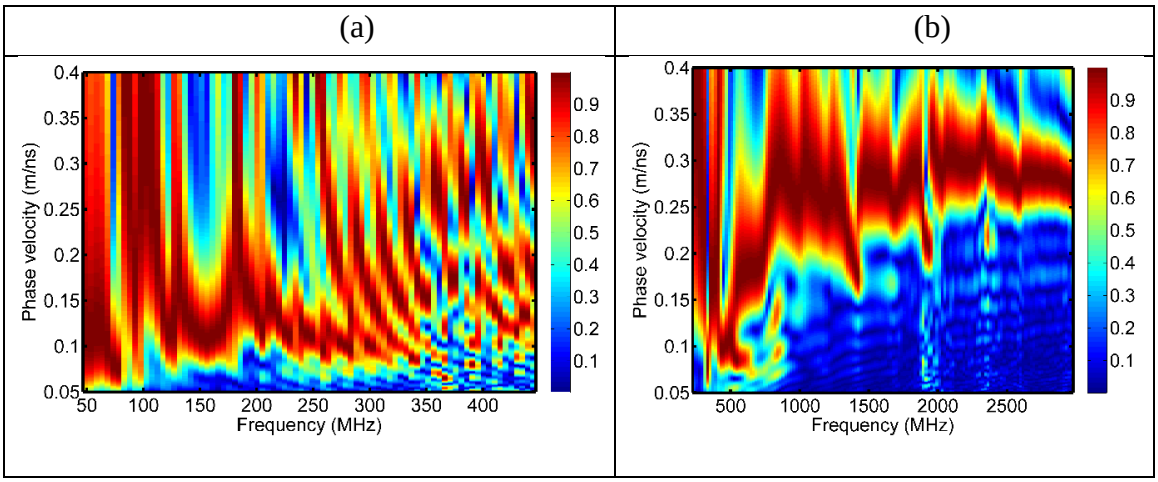

Figure 3.2. Dispersion images for experiment 2, (a) 100 MHz, and 33 cm overlying thickness. (b) 1000 MHz, and 18 cm overlying thickness.

High quality dispersion curves were most often observed in the 250 MHz and 500 MHz data Figure 3.3 shows higher quality dispersion curves for these frequencies. However, even with these frequencies, higher TE modes were not clearly defined. Although the higher TE modes were not well defined for 250 MHz (Figure 3.3.a), but for the 500 MHz frequency (Figure 3.3.b) the higher TE mode was clearly visible and well ranges.

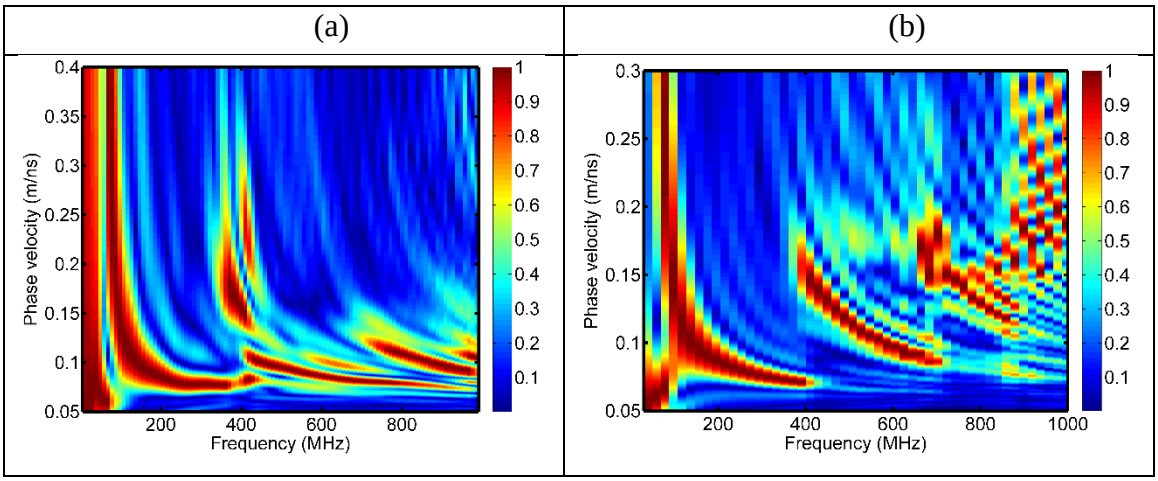

Figure 3.3. Dispersion images for experiment 2, (a) 250 MHz, and 9cm overlying thickness. (b) 500 MHz, and 9 cm overlying thickness.

3.3. ESTIMATION OF WAVEGUIDE THICKNESS

Using CMP surveys from all six experiments, the GPR data were inverted to estimate the thickness and permittivity of the overlying layer (the waveguide), as shown in Figures 3.4 and 3.5. To better visualize the differences that may be due to soil texture (instead of soil moisture, which controls permittivity), results from surveys acquired using a drier overlying layer (experiments 1, 3 and 5) are shown in Figure 3.4, while results from surveys acquired over a saturated overlying layer are shown in Figure 3.5. Of the surveys acquired over drier overlying layers, results from experiment 1 show the least correlation with the measured layer thickness, while experiments 3 and 5 show a consistent correlation.

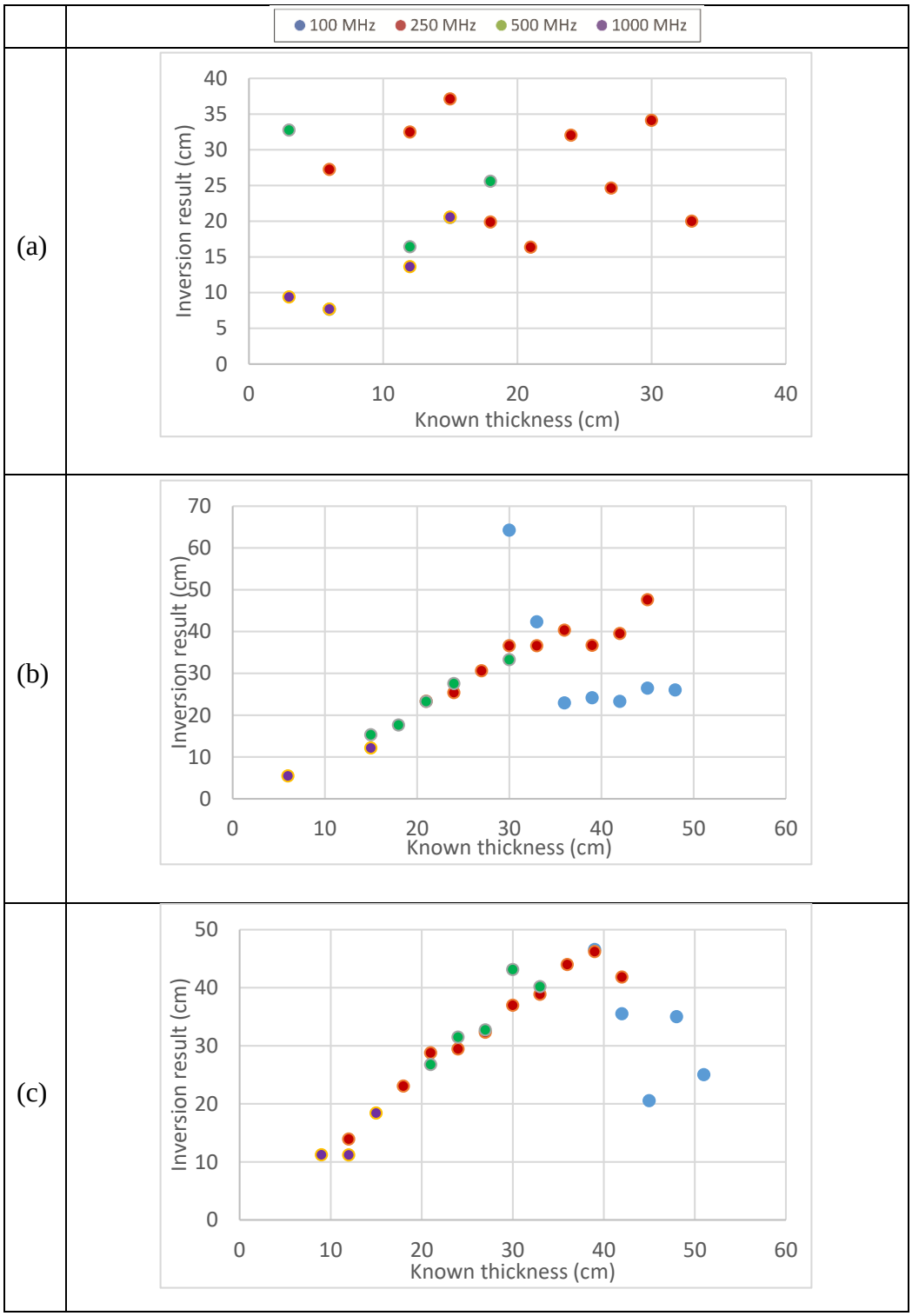

Figure 3.4. Estimated thickness (inversion) versus known overlying layer thickness for (a) Exp.1, (b) Exp.3, and (c) Exp.5.

For all three experiments, results from the 250 MHz and 500 MHz data best correlate with the measured layer thickness, while results from the 100 MHz data show little correlation. The 1000 MHz data show some correlation, but have very few surveys where dispersed waves formed sufficiently to allow inversion, so judging true correlation is difficult.

For surveys acquired over saturated overlying layers (Experiments 2, 4, and 6) only weak correlation is observed between estimated and measured layer thickness. Figure 3.5 displays no clear trend for any special soil texture nor for any frequency. However, the best correlation for these experiments is observed in the fairly linear correlation between the known and estimated layer thicknesses for 500 MHz frequency antenna acquired in experiment 2 when the overlying layer thicknesses ranges from 12 to 30 cm.

3.4. ANALYSIS OF ERROR: WAVEGUIDE THICKNESS ESTIMATION

Figures 3.6 and 3.7 quantify the thickness estimation errors as a function of known layer thickness. Figure 3.6 displays the error in the estimated thickness results for dry layers overlying a saturated basal layer (experiments 1, 3, and 5). As it can be seen, the error for the 100 MHz frequencies is very high, which is not surprising given the problems with data quality for this frequency. After the 100 MHz data are disregarded, the surveys with dry soil overlying wet organic soil (experiment 3) showed the least errors (Figure 3.6.b).

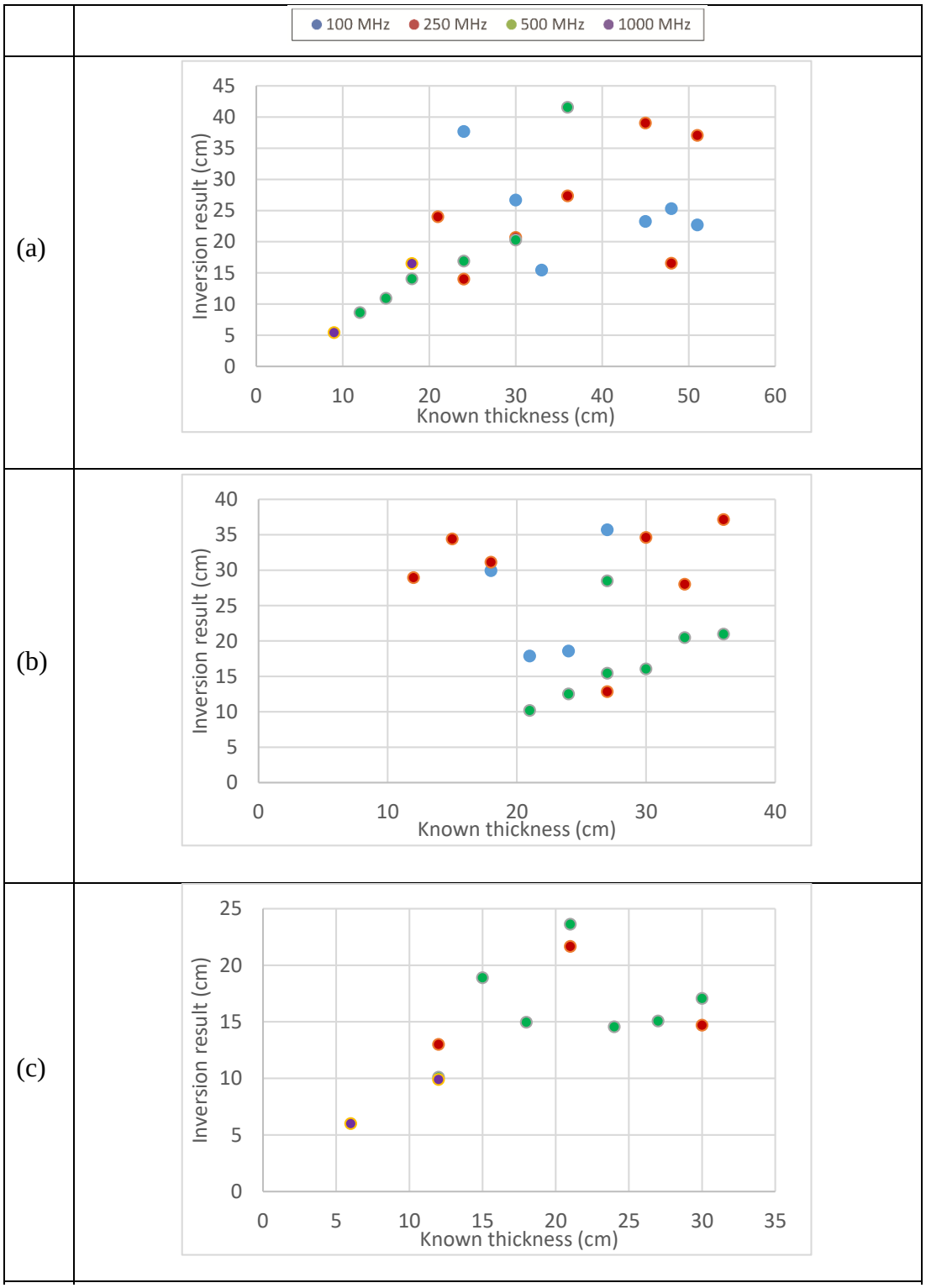

Figure 3.5. Estimated thickness (inversion) versus known overlying layer thickness for (a) Exp.2, (b) Exp.4, and (c) Exp.6.

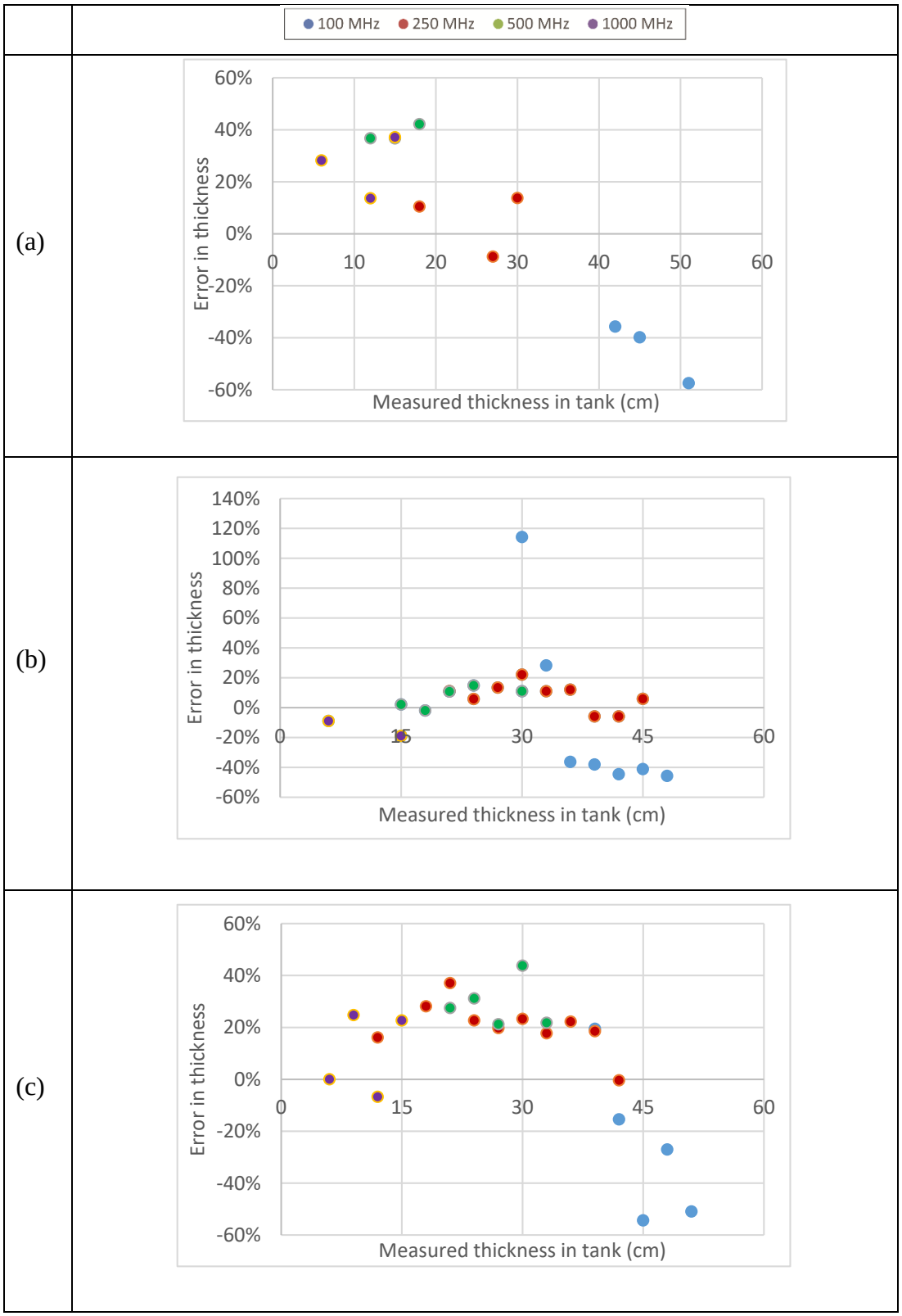

Figure 3.6. Error for GPR thickness measurements. (a) Exp.1, (b) Exp.3, and (c) Exp.5.

For experiments with a saturated surficial layer overlying a dry basal layer, the general trends in the errors shows that as the overlying soil thickness increased, the inversion results underestimated the thickness values, while inversion results tended to overestimate thickness when the overlying layer was thin. This is apparent in the organic soil, especially for the 500 MHz and 250 MHz data. Figure 3.7 shows the more random errors for the other two soil types (sands and silts), but still show an overall trend in estimation error.

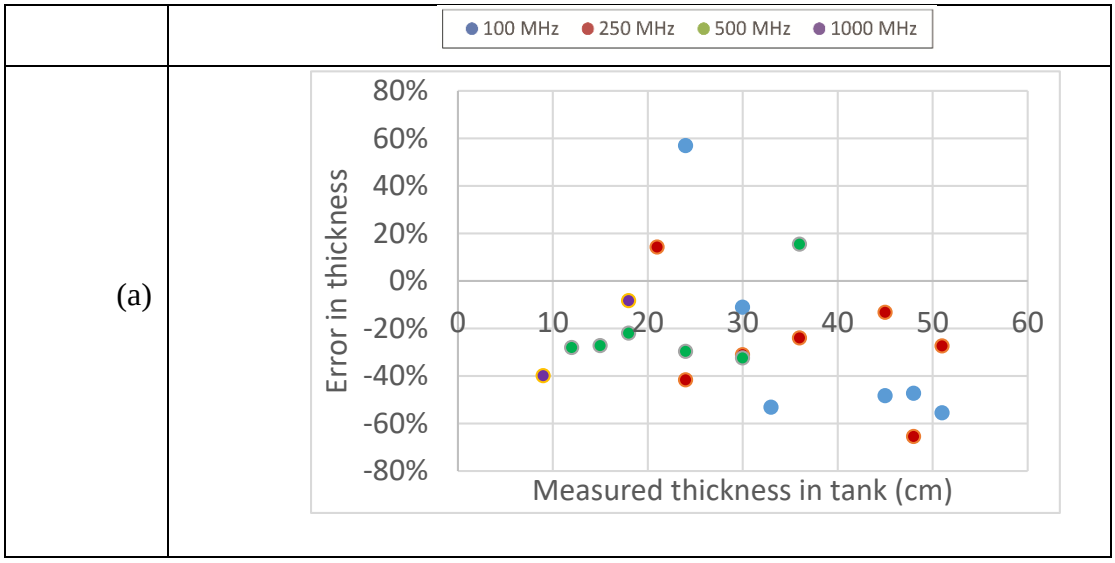

Figure 3.7. Error for GPR thickness measurements. (a) Exp.2, (b) Exp.4, and (c) Exp.6.

(b)

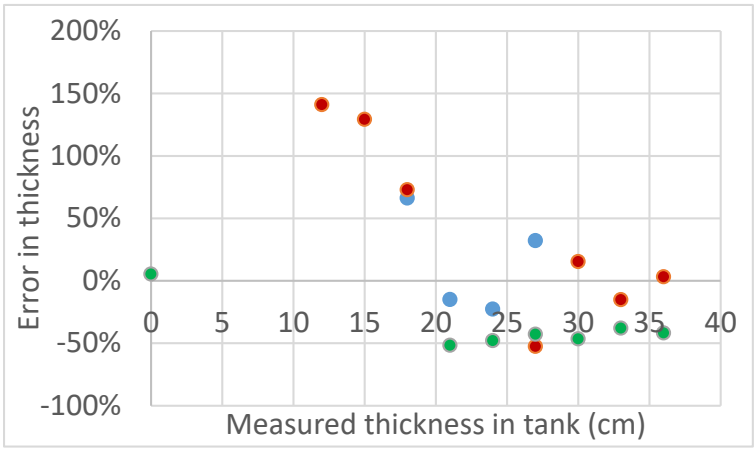

(c)

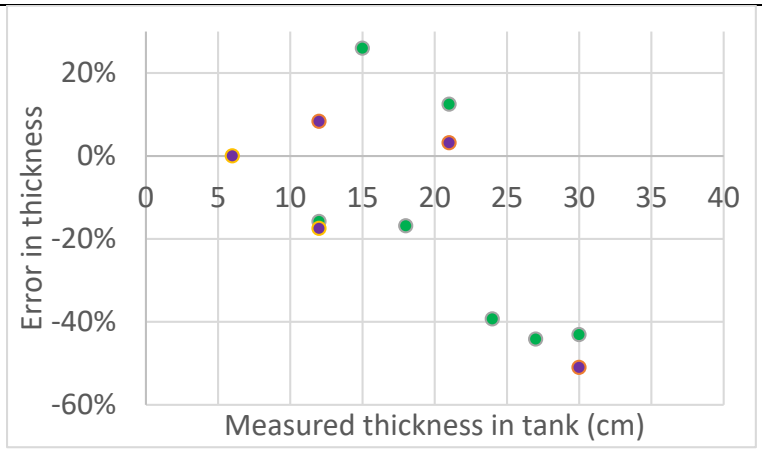

Figure 3.7. Error for GPR thickness measurements. (a) Exp.2, (b) Exp.4, and (c) Exp.6. (Cont.)

3.5. PERMITTIVITY ESTIMATION AND ANALYSIS OF ERROR

Next, the estimation-error in permittivity was analyzed as a function of the known permittivity (from TDR stations), frequency, soil texture, and thickness. As a matter of fact, Figures 3.8-3.10 confirm that the inversion results of the 250 and 500 MHz have the least errors among different soil textures and moisture contents. In addition, Figure 3.8.a,3.9.a, and 3.10.a reveal that 100 MHz frequency has the highest errors while the other three frequencies regress toward zero.

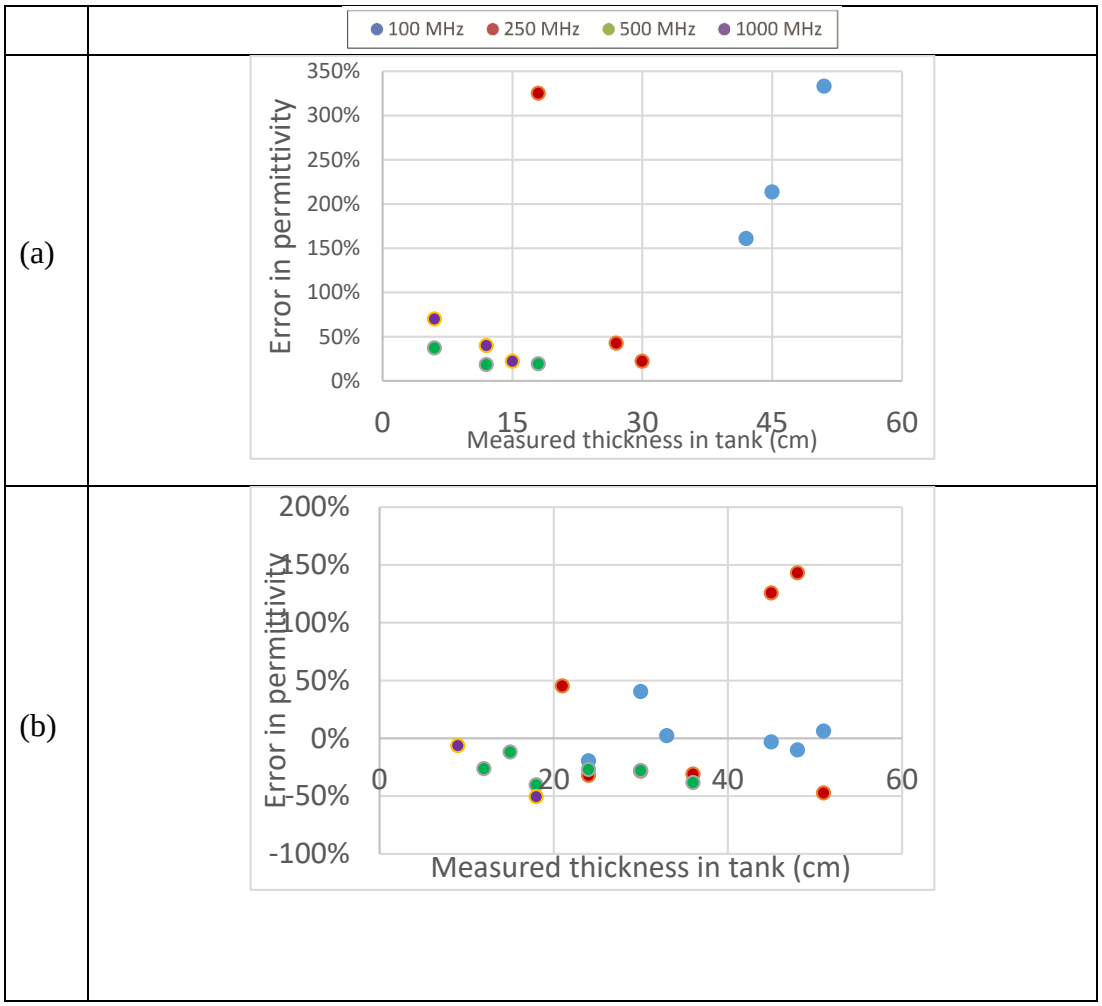

Figure 3.8. Error between GPR and measured permittivity as a function of known overlying layer thickness for (a) Exp. 1. (b) Exp. 2.

Moreover, figures 3.9.a and 3.10.a denote that, for organics and silts, when the drier layers were overlying wetter layers, the inversion method yielded the least errors in estimating the permittivities. Unlike organics and silts, sands indicated poor inversion results for permittivities, no matter what the moisture condition was for the experiment.

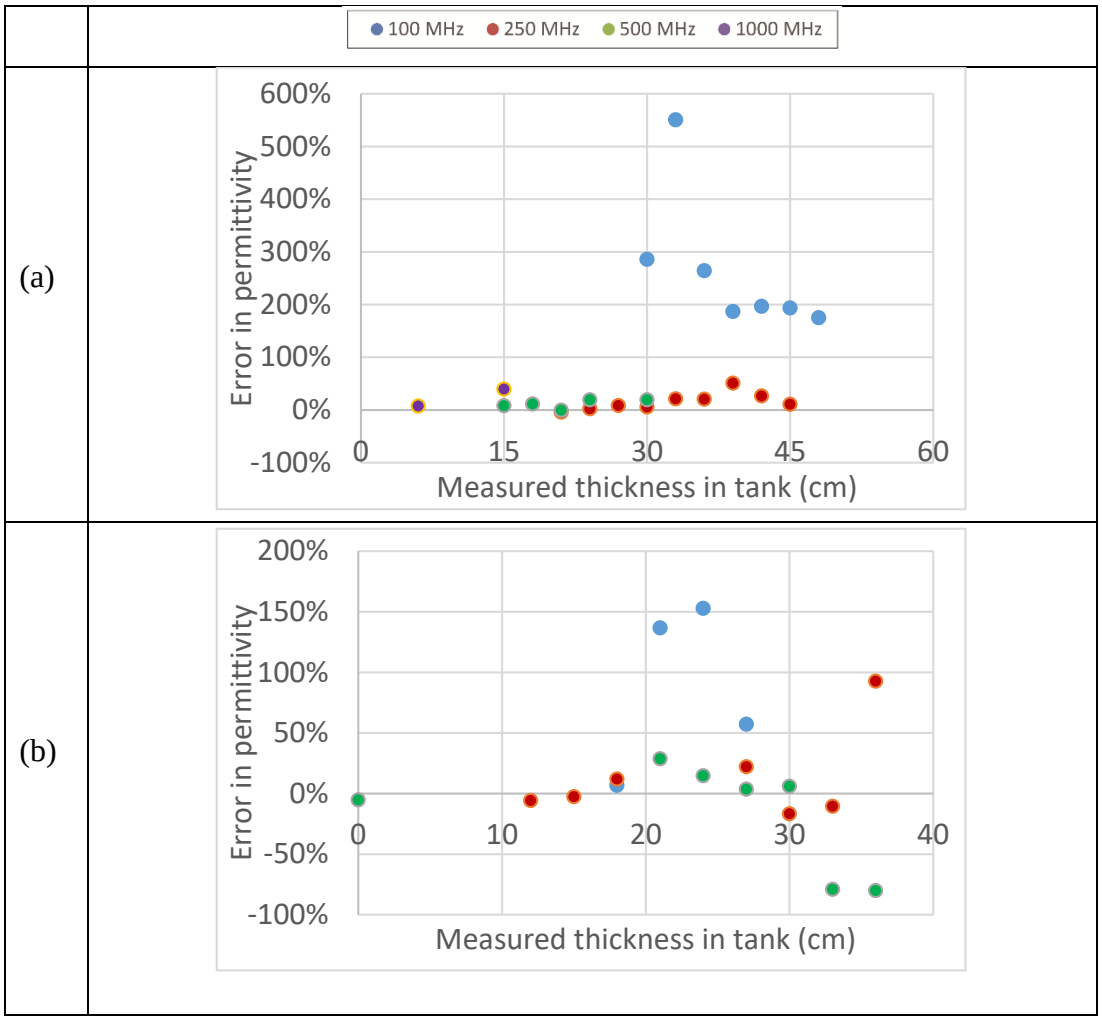

Figure 3.9. Error between GPR and measured permittivity as a function of known overlying layer thickness for (a) Exp. 3. (b) Exp. 4.

Moreover, figures 3.9.a and 3.10.a denote that, for organics and silts, when the drier layers were overlying wetter layers, the inversion method yielded the least errors in estimating the permittivities. Unlike organics and silts, sands indicated poor inversion results for permittivities, no matter what the moisture condition was for the experiment.

The results for the errors in estimated permittivites indicated that as the overlying thickness increased, the errors in the results increased as well.

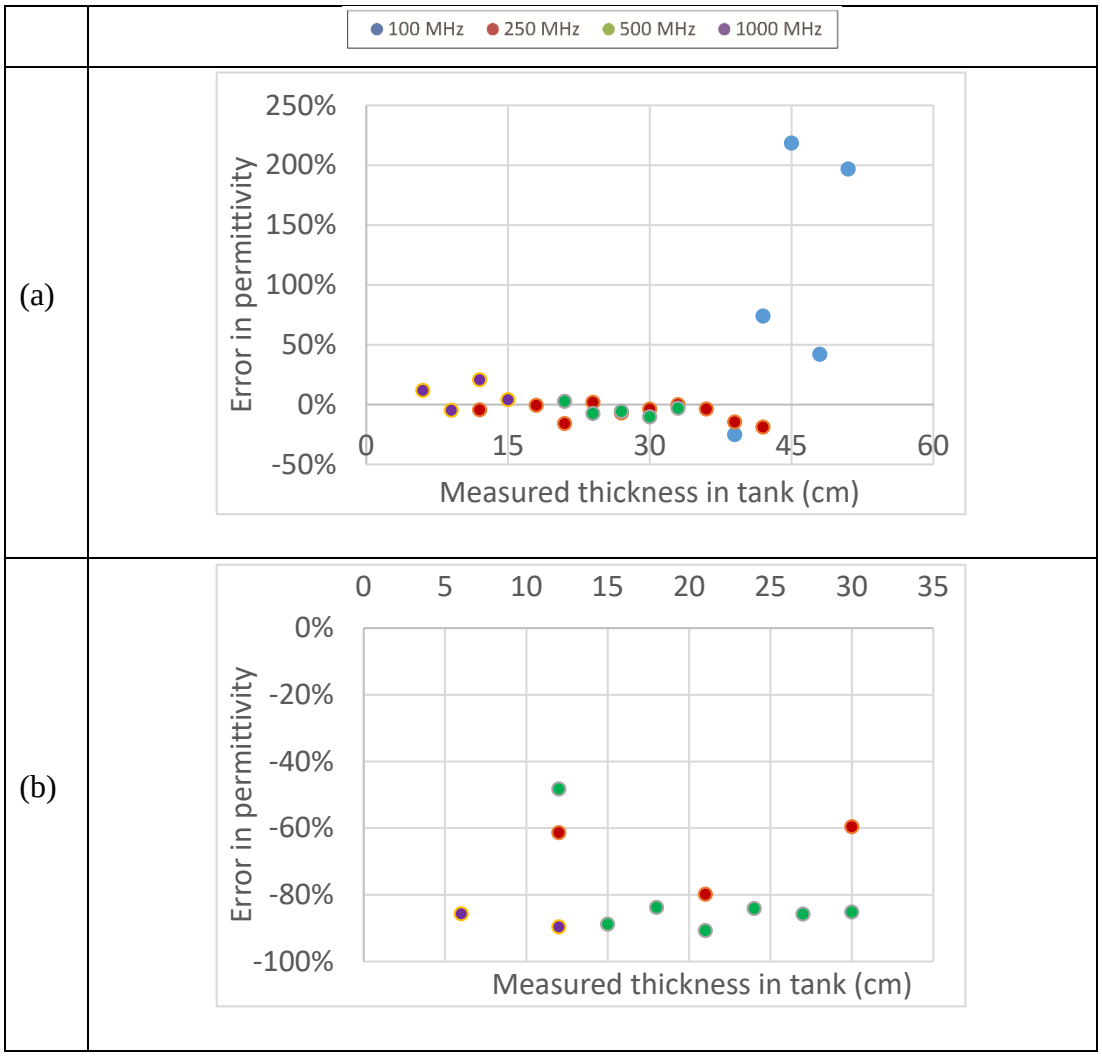

Figure 3.10. Error between GPR and measured permittivity as a function of known overlying layer thickness for (a) Exp. 5. (b) Exp. 6.

4. DISCUSSION

In the first place, because the layers in this study were homogenous and the geometric assumptions made for CMP and WARR are identical, it was expected that the CMP and WARR surveys yield the same results (identical dispersion images and inversions). The results shown in Figure 3.1 and Table 3.1 confirmed such expectancy. Previous study by van der Kruk [11] also underscored the same conclusion.

Second, it appeared from the GPR gathers and the dispersion images that that as the phase velocities and group velocities converged to the same value, less and less dispersion was noticed which confirms the result of the numerical study by Mangel et al. [7]. Generally speaking, the dispersion occurs when different frequency components of the electromagnetic wave propagate at different speeds, therefore, when the phase velocities (of different frequencies) converge to the same value (group velocity), less dispersion should be seen on the dispersion images.

Third, according to van der Kruk et al. [4], “the CMP measurements are not reliable as the phases cannot be clearly identified.” The results of this study also confirmed that CMP measurements can yield results with high errors both in layer thickness and permittivity estimations (especially in experiment 1). However, good results were obtained for the experiments with drier layers over wetter layers (leaky waveguides).

Fourth, as it was shown in Table 1, the inversion results for the 3 and 6 cm overlying layers are not satisfactory and great errors are seen. These poor results occur when the overlying layer is not yet sufficiently thick to develop a true guided waveform. The results of all experiments confirmed that there needs to be a minimum thickness for

the overlying layers before the waveguides fully formed. On the other hand, for the experiments 3 and 5, Figure 3.4.b and c show that after some thickness (40 cm) has been reached, the inversion of the dispersion curves resulted in high errors. Previous studies [1, 3, 14] suggested that a subsurface layer acts as waveguide only when its thickness is equal or less than the GPR wavelength. Therefore, the results of our experimental study confirm is in agreement with the results of previous studies.

Fifth, intermediate frequency surveys (250- and 500-MHz) appeared to be more accurate, at least for the leaky waveguides, where a layer of higher velocity lied over the basal layer of lower velocity (drier layers over wetter layer).

Sixth, higher frequencies resolved the physical properties of the waveguides better when the overlying layers where thinner, generally. This is again in agreement with the fact that the waveguide has to have a close or less thickness than the GPR wavelength. In fact, the dispersion images of this study indicated that as the thickness of the overlying layer increased, the dispersion images showed no or low quality curves for the high frequency GPR antennas.

Seventh, experiment 1 and 2 with the basal and overlying layers of sand showed irregular errors in permittivity and thickness estimation. However, compared with the other experiments, fewer data points in experiment 1 and 2 were available for the analysis.

5. CONCLUSIONS

In this study, six laboratory experiment with controlled environments were performed. A large tank was made and three different soil texture (sands, organics, and silts) were chosen. A basal layer of either drier or wetter soil were placed. Then thin layers (3cm) of contrasting soil moisture were added on top of the basal layer and GPR data were acquired using four different antenna frequencies (100-, 250-, 500-, and 1000-MHz). The results of this study indicated that the CMP and WARR acquisition methods appeared to yield similar results. In addition, it was concluded that for the very thin overlying layers (3 and 6 cm), it appeared that the waveguides were not fully formed. On the other hand, for the overlying layers of greater than 40 cm, the results indicated large errors, suggesting the fact that the overlying layer must have thickness of equal or less than the GPR wavelength. In addition, intermediate antenna frequencies of 250- and 500_MHz appeared to have more accurate results for the intermediate layers of 9 to 40 cm, especially when the drier overlying layers were places over the wetter basal layers.

ACKNOWLEDGEMENT

This project was supported by the National Research Initiative of the USDA Cooperative State Research, Education and Extension Service, grant number 2006-35107-17245 and by the University of Wisconsin-Eau Claire. This work was made possible by the great efforts of several undergraduates at University of Wisconsin-Eau Claire, and the authors would like to thank all their contributions.

REFERENCES

[1] S. A. Arcone, P. R. Peapples, and L. Liu, "Propagation of a ground-penetrating radar (GPR) pulse in a thin-surface waveguide," *Geophysics,* vol. 68, no. 6, pp. 1922-1933, 2003.

[2] K. Grote, T. Crist, and C. Nickel, "Experimental estimation of the GPR groundwave sampling depth," *Water Resources Research,* vol. 46, no. 10, 2010.

[3] S. A. Arcone, "Field observations of electromagnetic pulse propagation in dielectric slabs," *Geophysics,* vol. 49, no. 10, pp. 1763-1773, 1984.

[4] J. Van Der Kruk, S. A. Arcone, and L. Liu, "Fundamental and higher mode inversion of dispersed GPR waves propagating in an ice layer," *IEEE Transactions on Geoscience and Remote Sensing,* vol. 45, no. 8, pp. 2483-2491, 2007.

[5] J. Van Der Kruk, C. M. Steelman, A. L. Endres *et al.*, "Dispersion inversion of electromagnetic pulse propagation within freezing and thawing soil waveguides," *Geophysical Research Letters,* vol. 36, no. 18, 2009.

[6] J. Van der Kruk, R. W. Jacob, and H. Vereecken, "Properties of precipitation-induced multilayer surface waveguides derived from inversion of dispersive TE and TM GPR data," *Geophysics,* vol. 75, no. 4, pp. XWA263-WA273, 2010.

[7] A. R. Mangel, S. M. J. Moysey, and J. van der Kruk, "Resolving precipitation induced water content profiles by inversion of dispersive GPR data: A numerical study," *Journal of Hydrology,* vol. 525, pp. 496-505, June, 2015, 2015.

[8] J. van der Kruk, R. Streich, and A. G. Green, "Properties of surface waveguides derived from separate and joint inversion of dispersive TE and TM GPR data," *Geophysics,* vol. 71, no. 1, pp. K19-K29, 2006.

[9] J. van der Kruk, H. Vereecken, and R. W. Jcob, "Identifying dispersive GPR signals and inverting for surface wave-guide properties," *Leading Edge (Tulsa, OK),* vol. 28, no. 10, pp. 1234-1239, 2009.

[10] J. Bikowski, J. A. Huisman, J. A. Vrugt *et al.*, "Integrated analysis of waveguide dispersed GPR pulses using deterministic and Bayesian inversion methods," *Near Surface Geophysics,* vol. 10, no. 6, pp. 641- 652, December 2012, 2012.

[11] J. Van Der Kruk, "Properties of surface waveguides derived from inversion of fundamental and higher mode dispersive GPR data," *IEEE Transactions on Geoscience and Remote Sensing,* vol. 44, no. 10, pp. 2908-2915, 2006.

[12] F. S. Grant, and G. F. West, *Interpretation theory in applied geopysics*: McGraw-Hill Book Co, Inc., 1965.

[13] C. B. Park, R. D. Miller, and J. Xia, “Imaging dispersion curves of surface waves on multi-channel record,” in 68th Ann. Internat. Mtg., Soc. Expl. Geophys., 1998, pp. 1377-1380.

[14] L. Liu, and S. Arcone, “Numerical Simulation of the Wave-Guide Effect of the Near-Surface Thin Layer on Radar Wave Propagation,” *Journal of Environmental and Engineering Geophysics,* vol. 8, no. 2, pp. 133-141, 2003/06/01, 2003.

SECTION

2. CONCLUSIONS

First, the interaction of surface waves with the subsurface voids was studied. The results suggested that some range of frequencies in the surface waves were delayed while propagating through the air-filled voids. The location of these time delays identified the projected location of subsurface conduits/tunnels at various depths between 1.5 and 3.8 m.

Second, the attenuation analyses of surface waves due to presence of underground voids were studied. Different geophone frequencies were employed to acquire the shear wave component of Rayleigh waves and Love waves. Both Love waves and Rayleigh waves showed an anomaly in front of the location of the underground void. In addition, the time lapse technique was also tested using 100 Hz geophones. These experiments successfully identified the location of the buried conduit/underground voids. More numerical and experimental analyses are needed to study the effects of the size and embedment depth of the voids on the phase shifts of the surface wave frequency components.

Third, the dispersive characteristics of electromagnetic waves (GPR data) were studied to identify the thickness and permittivity of waveguides. A controlled soil environment was established in the lab. Six different experiments were carried out using three different soil textures (sands, organics, and silts) with varying moisture contents. Four different GPR antennas (100-, 250-, 500-, and 1000-MHz) were employed in the surveys. Generally, the two intermediate frequency surveys yielded the best results with the least errors. The experiments with the drier overlying layers were better characterized

by dispersive analysis of GPR data, which probably behaved as leaky waveguides. It is suggested for the future studies that the higher modes of the dispersion curves are taken into account for the inversion processing.

VITA

Payman Hajiani was born in Shiraz, Fars state, Iran. He received his Bachelor of Science degree in Physics in 2006 from the Islamic Azad University of Shiraz and Master of Science degree in Elementary Particle Physics in 2010 from the Ferdowsi University of Mashhad in Iran. In August 2011 Payman began his postgraduate studies in Geological/Geophysical Engineering at the Missouri University of Science and Technology under the supervision of Drs. Neil Anderson, J. David Rogers, and Katherine Grote. Since the spring semester of 2012 he has served in the Department of Geosciences and Geological and Petroleum Engineering as teaching and research assistant. Payman obtained his PhD in Geological/Geophysical Engineering from Missouri University of Science and Technology in December 2016.